

# Intelligent Reflecting Surface: Practical Phase Shift Model and Beamforming Optimization

Samith Abeywickrama, Rui Zhang, *Fellow, IEEE*, Qingqing Wu, *Member, IEEE*,

and Chau Yuen, *Senior Member, IEEE*

**Abstract**—Intelligent reflecting surface (IRS) that enables the control of wireless propagation environment has recently emerged as a promising cost-effective technology for boosting the spectral and energy efficiency of future wireless communication systems. Prior works on IRS are mainly based on the *ideal* phase shift model assuming full signal reflection by each of its elements regardless of the phase shift, which, however, is practically difficult to realize. In contrast, we propose in this paper a *practical* phase shift model that captures the *phase-dependent* amplitude variation in the element-wise reflection design. Based on the proposed model and considering an IRS-aided multiuser system with one IRS deployed to assist in the downlink communications from a multi-antenna access point (AP) to multiple single-antenna users, we formulate an optimization problem to minimize the total transmit power at the AP by jointly designing the AP transmit beamforming and the IRS reflect beamforming, subject to the users' individual signal-to-interference-plus-noise ratio (SINR) constraints. Iterative algorithms are proposed to find suboptimal solutions to this problem efficiently by utilizing the alternating optimization (AO) as well as penalty-based optimization techniques. Moreover, to draw essential insight, we analyze the *asymptotic performance loss* of the IRS-aided system that employs practical phase shifters but assumes the ideal phase shift model for beamforming optimization, as the number of IRS elements goes to infinity. Simulation results unveil substantial performance gains achieved by the proposed beamforming optimization based on the practical phase shift model as compared to the conventional ideal model.

**Index Terms**—Intelligent reflecting surface, passive array, beamforming optimization, phase shift model.

## I. INTRODUCTION

Intelligent reflecting surface (IRS) assisted wireless communication has recently emerged as a promising solution to enhance the spectral and energy efficiency of future wireless systems cost-effectively. Specifically, an IRS is able to establish favourable channel responses by controlling the wireless propagation environment via a large number of reconfigurable passive reflecting elements (see e.g. [2]–[6] and the references therein). In particular, it has been shown in [2] that when the number of reflecting elements, say  $N$ , is sufficiently large, IRS is able to achieve an asymptotic receive signal power or signal-to-noise ratio (SNR) gain of order  $\mathcal{O}(N^2)$  in the IRS-aided

Part of this work has been presented in the IEEE International Conference on Communications, Dublin, Ireland, 2020 [1].

S. Abeywickrama is with the Department of Electrical and Computer Engineering, National University of Singapore, Singapore, and also with Singapore University of Technology and Design, Singapore (e-mail: samith@u.nus.edu).

R. Zhang and Q. Wu are with the Department of Electrical and Computer Engineering, National University of Singapore, Singapore (e-mail: {elezhang,elewuqq}@nus.edu.sg).

C. Yuen is with Singapore University of Technology and Design, Singapore (e-mail: yuenchau@sutd.edu.sg).

single-user system, known as the *squared power gain*. Moreover, for the multiuser system, by jointly optimizing the active (transmit) beamforming at the base station and the passive (reflect) beamforming at the IRS, the signal-to-interference-plus-noise ratio (SINR) performance of all users in the network can be significantly improved [2], regardless of whether they are aided by the IRS directly or not. The proposed joint active and passive beamforming design has also been investigated in various other applications/setups, e.g., physical layer security [7]–[12], orthogonal frequency division multiplexing (OFDM) [13], [14], non-orthogonal multiple access (NOMA) [15], [16], and simultaneous wireless information and power transfer (SWIPT) [17]–[19]. However, the above prior works as well as many others (see, e.g., [20]–[29]) on IRS have all assumed the ideal phase shift model with full signal reflection, i.e., unity reflection amplitude at each reflecting element regardless of its phase shift, which, however, is practically difficult to realize due to the hardware limitation [30], [31].

The *amplitude response* of a typical passive reflecting element is generally non-uniform with respect to its phase shift. In particular, the amplitude typically exhibits its minimum value at the zero phase shift, but monotonically increases and asymptotically approaches unity amplitude at the phase shift of  $\pi$  or  $-\pi$ . This is due to the fact that when the phase shift approaches zero, the image currents, i.e., the currents of a virtual source that accounts for the reflection, are in-phase with the reflecting element currents, thus the electric field and the current flow in each element are enhanced. As a result, the dielectric loss, metallic loss, and ohmic loss increase accordingly, leading to more energy loss and hence lower reflection amplitude [30]. Furthermore, these losses mainly come from the semiconductor devices, metals, and dielectric substrates in IRS, thus cannot be completely avoided in practice. In fact, this is a long-standing problem for designing reflection-based metasurfaces [32]. In [33], amplifiers are integrated into the reflecting elements to compensate the energy loss, which, however, is unsuitable for passive IRS and also costly to implement in practice.

In prior works (e.g., [7]–[29]) on IRS, by assuming the ideal phase shift model with unity reflection amplitude regardless of the phase shift at each element, IRS reflection has been designed to achieve the maximal phase alignment between the IRS-reflected and non-IRS-reflected signals at the designated receiver(s). However, when the reflection amplitude depends on the phase shift, such a reflection design is no longer optimal in general and will cause performance degradation. Instead, the phase shifts at the IRS need to be properly designed to strike

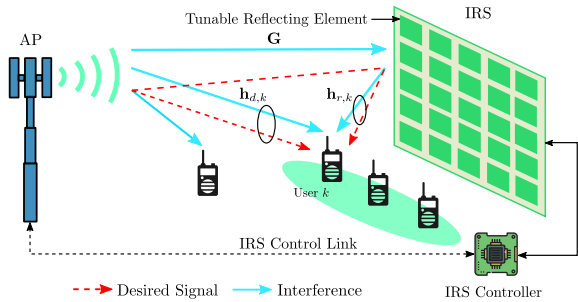


Fig. 1: An IRS-aided multiuser wireless communication system.

an optimal balance between the reflected signal amplitude (by each element) and phase alignment (over all the elements) under the practical phase shift model with phase-dependent amplitude response, which, however, cannot be accomplished by directly applying the existing models of IRS and thus motivates this work.

In this paper, by establishing a practical IRS phase shift model and considering an IRS-aided multiuser wireless communication system shown in Fig. 1, we formulate and solve new problems to minimize the total transmit power at the access point (AP) by jointly optimizing the AP transmit beamforming and the IRS reflect beamforming, subject to the users' individual SINR constraints. Our main contributions are summarized as follows.

- First, to characterize the fundamental relationship between the reflection amplitude and phase shift for designing IRS-aided wireless systems, we propose a new *analytical model* for the phase shifter, which is applicable to a variety of semiconductor devices used for implementing IRS, and verify its accuracy using the experimental results from the existing literature.
- Next, based on the newly established phase shift model, we solve the formulated problem for the special case of single-user transmission to draw useful design insights. However, the problem in this case is non-convex and difficult to be optimally solved in general, for which we propose two iterative algorithms to find suboptimal solutions efficiently by utilizing the alternating optimization (AO) and penalty-based optimization techniques, respectively. Moreover, to highlight the importance of the practical phase shift model, we analyze the asymptotic performance loss of an IRS-aided system that employs practical phase shifters but assumes the ideal phase shift model for beamforming optimization, as the number of IRS elements becomes large.
- Finally, we extend our formulated problem for the single-user case to the general multiuser case and propose two algorithms to obtain suboptimal solutions for it, which offer different tradeoffs between the complexity and performance. Specifically, the first algorithm, which is based on the penalty-based method, achieves better performance but requires higher complexity as compared to the second algorithm, which is designed by following the similar principle of two-stage optimization as proposed in [2]. Simulation results unveil substantial performance

gains achieved by the proposed beamforming optimization based on the practical phase shift model as compared to the conventional ideal model, although the latter has been widely adopted in the literature.

The rest of this paper is organized as follows. Section II introduces the system model. Section III presents the proposed practical IRS phase shift model. Section IV presents the problem formulation for the single-user case and proposes two efficient algorithms to solve the problem. In Section V, we extend the algorithms proposed for the single-user case to the general multiuser case. Section VI presents numerical results to evaluate the effectiveness of the proposed algorithms. Finally, we conclude the paper in Section VII.

*Notations:* In this paper, scalars are denoted by italic letters, vectors and matrices are denoted by bold-face lower-case and upper-case letters, respectively. For a complex-valued vector  $\mathbf{v}$ ,  $\|\mathbf{v}\|$ ,  $\mathbf{v}^H$ , and  $\text{diag}(\mathbf{v})$  denote its  $\ell_2$ -norm, conjugate transpose, and a diagonal matrix with each diagonal element being the corresponding element in  $\mathbf{v}$ , respectively. Scalar  $v_i$  denotes the  $i$ -th element of a vector  $\mathbf{v}$ . For a square matrix  $\mathbf{S}$ ,  $\text{Tr}(\mathbf{S})$  and  $\mathbf{S}^{-1}$  denote its trace and inverse, respectively, while  $\mathbf{S} \succeq 0$  means that  $\mathbf{S}$  is positive semi-definite. For any matrix  $\mathbf{A}$ ,  $\mathbf{A}^H$ ,  $\text{rank}(\mathbf{A})$ , and  $\mathbf{A}_{n,k}$  denote its conjugate transpose, rank, and  $(n, k)$ th element, respectively.  $\mathbf{I}$  and  $\mathbf{0}$  denote an identity matrix and an all-zero matrix, respectively, with appropriate dimensions.  $\mathbb{C}^{x \times y}$  denotes the space of  $x \times y$  complex-valued matrices.  $j$  denotes the imaginary unit, i.e.,  $j^2 = -1$ . For a complex-valued scalar  $v$ ,  $|v|$  and  $\arg(v)$  denote its absolute value and phase, respectively. The distribution of a circularly symmetric complex Gaussian (CSCG) random vector with mean  $\mu$  and variance  $\varrho^2$  is denoted by  $\mathcal{CN}(\mu, \varrho^2)$ ; and  $\sim$  stands for “distributed as”.  $\mathbb{E}(\cdot)$  denotes the statistical expectation.

## II. SYSTEM MODEL

As shown in Fig. 1, we consider a multiuser multiple-input single-output (MISO) wireless system, where an IRS composed of  $N$  reflecting elements is deployed to assist in the downlink communications from an AP with  $M$  antennas to  $K$  single-antenna users. The set of the users is denoted by  $\mathcal{K} = \{1, \dots, K\}$ . The IRS reflecting elements are programmable via a smart IRS controller [3]. Furthermore, the IRS controller communicates with the AP via a separate wireless link for the AP to control the IRS reflection. It is assumed that the signals that are reflected by the IRS more than once have negligible power due to substantial path loss and thus are ignored [2]. In addition, we consider a quasi-static flat-fading model, where it is assumed that all the wireless channels remain constant over each transmission block. All the channels are assumed to be known at the AP by applying, e.g., the channel estimation techniques proposed in [3], [14].

Let  $\mathbf{h}_{d,k} \in \mathbb{C}^{M \times 1}$ ,  $\mathbf{h}_{r,k} \in \mathbb{C}^{N \times 1}$ , and  $\mathbf{G} \in \mathbb{C}^{N \times M}$  denote the baseband equivalent channels from the AP to user  $k$ , from the IRS to user  $k$ , and from the AP to IRS, respectively,  $k \in \mathcal{K}$ . Without loss of generality, let  $\mathbf{v} = [v_1, \dots, v_N] \in \mathbb{C}^{N \times 1}$  denote the reflection coefficient vector of the IRS, where  $|v_n| \in [0, 1]$  and  $\arg(v_n) \in [-\pi, \pi]$  are the reflection

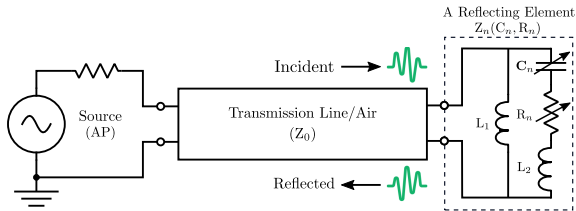


Fig. 2: Transmission line model of a reflecting element.

amplitude and phase shift on the combined incident signal, respectively, for  $n \in \{1, \dots, N\}$  [3]. Note that for the ideal phase shift model considered in [2]–[4], it follows that  $|v_n| = 1, \forall n$ , regardless of the phase shift,  $\arg(v_n)$ . The transmit signal at the AP is given by  $\mathbf{x} = \sum_{k=1}^K \mathbf{w}_k s_k$ , where  $\mathbf{w}_k \in \mathbb{C}^{M \times 1}$  denotes the transmit beamforming vector for user  $k$  and  $s_k$  denotes the corresponding transmit symbol, which is independent over  $k$ , and has zero-mean and unit-variance (i.e.,  $\mathbb{E}(|s_k|^2) = 1$ ). The signal received at user  $k$  from both the AP-user and AP-IRS-user channels is then expressed as

$$y_k = (\mathbf{v}^H \Phi_k + \mathbf{h}_{d,k}^H) \sum_{j=1}^K \mathbf{w}_j s_j + z_k, k \in \mathcal{K}, \quad (1)$$

where  $\Phi_k = \text{diag}(\mathbf{h}_{r,k}^H) \mathbf{G}$  and  $z_k$  denotes the additive white Gaussian noise (AWGN) at the user  $k$ 's receiver with zero-mean and variance  $\sigma_k^2$ . Accordingly, the SINR of user  $k$  is given by

$$\text{SINR}_k = \frac{|(\mathbf{v}^H \Phi_k + \mathbf{h}_{d,k}^H) \mathbf{w}_k|^2}{\sum_{j \neq k}^K |(\mathbf{v}^H \Phi_k + \mathbf{h}_{d,k}^H) \mathbf{w}_j|^2 + \sigma_k^2}, k \in \mathcal{K}. \quad (2)$$

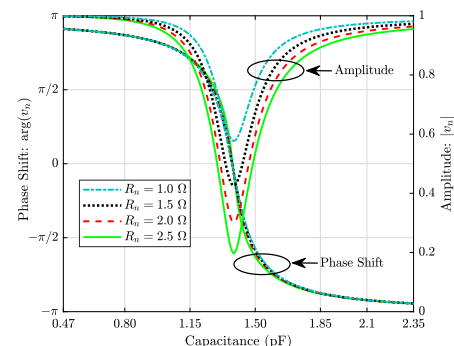
### III. PRACTICAL PHASE SHIFT MODEL

#### A. Equivalent Circuit Model

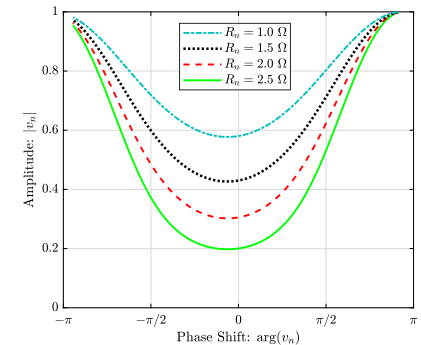
An IRS is typically constructed by using the printed circuit board (PCB), where the reflecting elements are equally spaced on a two-dimensional plane. A reflecting element is composed of a metal patch on the top layer of the PCB dielectric substrate and a full metal sheet on the bottom layer [3]. Moreover, a semiconductor device<sup>1</sup>, which can vary the impedance of the reflecting element by controlling its biasing voltage, is embedded into the top layer metal patch so that the element response can be dynamically tuned in real time without changing the geometrical parameters [35]. In other words, when the geometrical parameters are fixed, the semiconductor device controls the phase shift and reflection amplitude (absorption level).

As the physical length of a reflecting element is usually smaller than the wavelength of the desired incident signal, its response can be accurately described by an equivalent lumped circuit model regardless of the particular geometry of the element [36]. As such, the metallic parts in the reflecting element can be modeled as inductors as the high-frequency current flowing in it produces a quasi-static magnetic field. In

<sup>1</sup>In practice, a positive-intrinsic-negative (PIN) diode, a variable capacitance (varactor) diode, or a metal-oxide-semiconductor field-effect transistor (MOSFET) can be used as the semiconductor device mentioned here [32], [34], [35].



(a) Phase shift and amplitude versus  $C_n$  and  $R_n$ .



(b) Amplitude versus phase shift.

Fig. 3: Reflection coefficient of a reflecting element.

Fig. 2, the equivalent model for the  $n$ -th reflecting element is illustrated as a parallel resonant circuit and its impedance is given by

$$Z_n(C_n, R_n) = \frac{j\omega L_1(j\omega L_2 + \frac{1}{j\omega C_n} + R_n)}{j\omega L_1 + (j\omega L_2 + \frac{1}{j\omega C_n} + R_n)}, \quad (3)$$

where  $L_1$ ,  $L_2$ ,  $C_n$ ,  $R_n$ , and  $\omega$  denote the bottom layer inductance, top layer inductance, effective capacitance, effective resistance, and angular frequency of the incident signal, respectively. Note that  $R_n$  determines the amount of power dissipation due to the losses in the semiconductor devices, metals, and dielectrics, which cannot be zero in practice, and  $C_n$  specifies the charge accumulation related to the element geometry and semiconductor device. As the transmission line diagram in Fig. 2 depicts, the reflection coefficient, i.e.,  $v_n$  in (1), is the parameter that describes the fraction of the reflected electromagnetic wave due to the impedance discontinuity between the free space impedance  $Z_0$  and element impedance  $Z_n(C_n, R_n)$  [37], which is given by

$$v_n = \frac{Z_n(C_n, R_n) - Z_0}{Z_n(C_n, R_n) + Z_0}. \quad (4)$$

Since  $v_n$  is a function of  $C_n$  and  $R_n$ , the reflected electromagnetic waves can be manipulated in a controllable and programmable manner by varying  $C_n$ 's and  $R_n$ 's.

To demonstrate this, Fig. 3 illustrates the behaviour of the amplitude and the phase shift, i.e.,  $|v_n|$  and  $\arg(v_n)$ , respectively, for different values of  $C_n$  and  $R_n$ . Note that to align with the experimental results in [32],  $C_n$  is varied from 0.47 pF to 2.35 pF when  $L_1 = 2.5$  nH,  $L_2 = 0.7$  nH,

$Z_0 = 377 \Omega$ , and  $\omega = 2\pi \times 2.4 \times 10^9$ . It is observed that although a reflecting element is capable of achieving almost  $2\pi$  full phase tuning, its phase shift and reflection amplitude both vary with  $C_n$  and  $R_n$  in general. One can also observe that the minimum amplitude occurs near zero phase shift and approaches unity (the maximum value) at the phase shift of  $\pi$  or  $-\pi$ , which is explained as follows. When the phase shift is around  $\pi$  or  $-\pi$ , the reflective currents (also termed as image currents) are out-of-phase with the element currents, and thus the electric field as well as the current flow in the element are both diminished, thus resulting in minimum energy loss and the highest reflection amplitude. In contrast, when the phase shift is around zero, the reflective currents are in-phase with the element currents, and thus the electric field as well as the current flow in the element are both enhanced. As a result, the dielectric loss, metallic loss, and ohmic loss increase dramatically, leading to maximum energy dissipation and the lowest reflection amplitude. Furthermore, it is worth pointing out that the numerical results illustrated in Fig. 3 are in accordance with the experimental results reported in the literature (see [30] and Fig. 5 (b) in [32]), indicating that the circuit model given by (3) and (4) accurately captures the physical reflection of a reflecting element in practice.

Note that to obtain the ideal phase shift control, where  $|v_n| = 1, \forall \arg(v_n) \in [-\pi, \pi]$ , each element should exhibit zero energy dissipation for reflection. However, in practical hardware, energy dissipation is unavoidable<sup>2</sup> and the typical behaviour of the reflection amplitude is similar to Fig. 3. Therefore, incorporating the practical phase shift model to design beamforming algorithms is essential to optimize the performance of IRS-aided wireless systems.

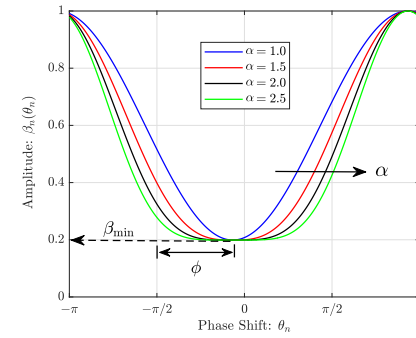
### B. Proposed Phase Shift Model

In order to characterize the fundamental relationship between the reflection amplitude and phase shift for designing IRS-aided wireless systems, we propose in this subsection an analytical model for the phase shift which is in general applicable to a variety of semiconductor devices used for implementing IRS. Let  $v_n = \beta_n(\theta_n)e^{j\theta_n}$  with  $\theta_n \in [-\pi, \pi]$  and  $\beta_n(\theta_n) \in [0, 1]$  respectively denote the phase shift and the corresponding amplitude. Specifically,  $\beta_n(\theta_n)$  can be expressed as

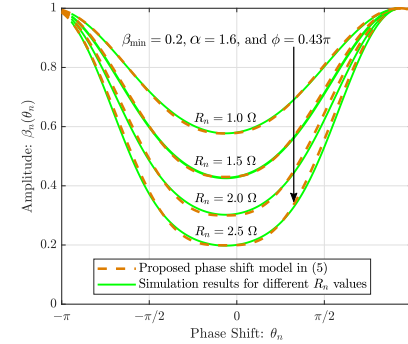
$$\beta_n(\theta_n) = (1 - \beta_{\min}) \left( \frac{\sin(\theta_n - \phi) + 1}{2} \right)^\alpha + \beta_{\min}, \quad (5)$$

where  $\beta_{\min} \geq 0$ ,  $\phi \geq 0$ , and  $\alpha \geq 0$  are the constants related to the specific circuit implementation. As depicted in Fig. 4 (a),  $\beta_{\min}$  is the minimum amplitude,  $\phi$  is the horizontal distance between  $-\pi/2$  and  $\beta_{\min}$ , and  $\alpha$  controls the steepness of the function curve. Note that for  $\beta_{\min} = 1$  (or  $\alpha = 0$ ), (5) is equivalent to the ideal phase shift model with unity amplitude. In practice, IRS circuits are fixed once they are fabricated and thus these parameters can be easily found by a standard curve fitting tool.

<sup>2</sup>In [32],  $R_n = 2.5 \Omega$  in each reflecting element due to the diode junction resistance, while in [30], although the reflecting element does not contain any semiconductor device, its amplitude response follows a similar shape to Fig. 3 due to the metallic loss and dielectric loss.



(a) The phase shift model with different parameters.



(b) Simulation results for the proposed phase shift model.

Fig. 4: The proposed phase shift model.

Fig. 4 (b) illustrates that the proposed phase shift model closely matches the simulation results presented in Section III-A for a practical reflecting element. In the sequel, we will adopt the model in (5) for beamforming design in IRS-aided wireless communication. Without loss of generality, we assume that the circuits of the reflecting elements are all identical, and thus the same model parameters, i.e.,  $\beta_{\min}$ ,  $\phi$ , and  $\alpha$ , apply to each of the elements at the IRS.

## IV. SINGLE-USER BEAMFORMING OPTIMIZATION

In this section, we consider the special case with a single user to draw important insights into the beamforming design. For brevity, the user index  $k$  is omitted in this section.

### A. Problem Formulation

We aim to minimize the total transmit power at the AP by jointly optimizing the transmit beamforming at the AP and reflect beamforming at the IRS for  $K = 1$ . In this case, no inter-user interference is present in (2), and thus the problem is formulated as

$$(P0) : \min_{\mathbf{w}, \mathbf{v}, \{\theta_n\}} \|\mathbf{w}\|^2 \quad (6)$$

$$\text{s.t. } |(\mathbf{v}^H \Phi + \mathbf{h}_d^H) \mathbf{w}|^2 \geq \gamma \sigma^2, \quad (7)$$

$$v_n = \beta_n(\theta_n) e^{j\theta_n}, n = 1, \dots, N, \quad (8)$$

$$-\pi \leq \theta_n \leq \pi, n = 1, \dots, N, \quad (9)$$

where  $\gamma > 0$  is the minimum SNR requirement of the user. Although the objective function of (P0) and constraints in

(9) are convex, it is challenging to solve (P0) due to the non-convex constraints in (7) and (8). For any given  $\mathbf{v}$  and  $\{\theta_n\}_{n=1}^N$ , it is not difficult to verify that the maximum-ratio transmission (MRT) is the optimal transmit beamforming solution to (P0), i.e.,  $\mathbf{w}^* = \sqrt{P} \frac{(\mathbf{v}^H \Phi + \mathbf{h}_d^H)^H}{\|\mathbf{v}^H \Phi + \mathbf{h}_d^H\|}$  [2], where  $P$  denotes the transmit power of the AP. By substituting  $\mathbf{w}^*$  to (P0), the problem can be transformed to

$$\min_{P, \mathbf{v}, \{\theta_n\}} P \quad (10)$$

$$\text{s.t. } P \|\mathbf{v}^H \Phi + \mathbf{h}_d^H\|^2 \geq \gamma \sigma^2, \quad (11)$$

$$v_n = \beta_n(\theta_n) e^{j\theta_n}, n = 1, \dots, N, \quad (12)$$

$$-\pi \leq \theta_n \leq \pi, n = 1, \dots, N, \quad (13)$$

where the optimal transmit power is given by  $P^* = \frac{\gamma \sigma^2}{\|\mathbf{v}^H \Phi + \mathbf{h}_d^H\|^2}$ . Accordingly, the problem for minimizing the total transmit power at the AP by optimizing  $\mathbf{v}$  and  $\{\theta_n\}_{n=1}^N$  can be equivalently formulated as

$$(P1) : \max_{\mathbf{v}, \{\theta_n\}} \|\mathbf{v}^H \Phi + \mathbf{h}_d^H\|^2 \quad (14)$$

$$\text{s.t. } v_n = \beta_n(\theta_n) e^{j\theta_n}, n = 1, \dots, N, \quad (15)$$

$$-\pi \leq \theta_n \leq \pi, n = 1, \dots, N. \quad (16)$$

It is worth noting that (P1) essentially corresponds to the effective channel power gain maximization for the single user. Although simplified, problem (P1) is still non-convex and difficult to be optimally solved due to the non-convex constraints in (15).

### B. Power Loss of Ideal IRS Model with Large $N$

Prior to solving (P1), in this subsection, we first characterize the receive power loss in a practical IRS-aided system when the phase shifts are designed by assuming the ideal phase shift model, i.e., by setting  $\beta_n(\theta_n) = 1, \forall n$  in (15), as the number of IRS elements  $N \rightarrow \infty$ . Since the IRS-reflected signal power dominates in the total received power for asymptotically large  $N$ , the signal received from the AP-user link is ignored. To draw essential insight, we assume a single-antenna transmitter at the AP, i.e.,  $M = 1$ , with the transmit power denoted by  $P$ . Denote by  $P_{\text{ideal}}$  and  $P_{\text{practical}}$  the receive power under the ideal and practical IRS phase shift models, respectively, with the phase shifts obtained by solving (P1) by assuming the ideal IRS model, i.e.,  $\beta_n(\theta_n) = 1, \forall n$  in (15).

*Proposition 1:* Assume that  $\mathbf{h}_r(n) \sim \mathcal{CN}(0, \varrho_g^2)$  and  $\mathbf{G}(n, 1) \sim \mathcal{CN}(0, \varrho_g^2), n = 1, \dots, N$ , and they are statistically independent. As  $N \rightarrow \infty$ , we have

$$\eta(\beta_{\min}, \alpha) = \frac{P_{\text{practical}}}{P_{\text{ideal}}} = \left( \frac{1}{2\pi} \int_{-\pi}^{\pi} \beta(\theta) d\theta \right)^2, \quad (17)$$

where  $\beta(\theta) = (1 - \beta_{\min}) \left( \frac{\sin(\theta - \phi) + 1}{2} \right)^\alpha + \beta_{\min}$ .

*Proof:* See Appendix A. ■

From (17), it is observed that as  $N \rightarrow \infty$ , the power ratio  $\eta(\beta_{\min}, \alpha)$  depends only on  $\beta_{\min}$  and  $\alpha$ , but is regardless of  $N$ , which implies that the promising squared power scaling order, i.e.,  $\mathcal{O}(N^2)$  unveiled in [2] under the ideal phase shift model, still holds for practical phase shifters. Besides, it is

TABLE I: The Power Loss Under Ideal IRS Assumption.

$\eta(\beta_{\min}, \alpha)$	$\beta_{\min} = 1.0$	$\beta_{\min} = 0.8$	$\beta_{\min} = 0.5$	$\beta_{\min} = 0.2$
$\alpha = 1.6$	0 dB	-1.1 dB	-3.0 dB	-5.5 dB
$\alpha = 2.0$	0 dB	-1.2 dB	-3.2 dB	-6.0 dB

observed from the numerical values in Table I that  $\eta(\beta_{\min}, \alpha)$  is more sensitive to  $\beta_{\min}$  as compared to  $\alpha$ . For example, when  $\beta_{\min} = 0.2$  and  $\alpha = 1.6$  (which correspond to the setup in [32]), a substantial power loss of 5.5 dB is incurred under the ideal IRS assumption. Even for a much larger value of  $\beta_{\min}$ , the power loss is still non-negligible, e.g.,  $\eta(0.8, 1.6) = -1.1$  dB. These results suggest that the consideration of IRS hardware imperfection is indeed crucial for the beamforming design and achievable performance in practical systems. To this end, we solve (P1) in the next two subsections under the proposed practical phase shift model by applying two different optimization techniques, respectively.

### C. AO-based Algorithm

First, we propose an AO-based algorithm to find an approximate solution to (P1), by iteratively optimizing one phase shift of the  $N$  reflecting elements with those of the others being fixed at each time, until the objective value in (14) converges. To this end, the problem for optimizing the reflection of the  $n$ -th element is simplified to

$$(P2) : \max_{\theta_n} \beta_n^2(\theta_n) \Psi_{n,n} + \beta_n(\theta_n) |\varphi_n| \cos(\arg(\varphi_n) - \theta_n) \quad (18)$$

$$\text{s.t. } -\pi \leq \theta_n \leq \pi, \quad (19)$$

where  $\Psi = \text{diag}(\mathbf{h}_r^H) \mathbf{G} \mathbf{G}^H \text{diag}(\mathbf{h}_r)$ ,  $\hat{\mathbf{h}}_d = \text{diag}(\mathbf{h}_r^H) \mathbf{G} \mathbf{h}_d$ , and  $\varphi_n = (\sum_{m \neq n}^N \Psi_{n,m} v_m) + 2\hat{h}_{d,n}$ . Note that (18) is obtained by taking the terms associated with  $\beta_n(\theta_n)$  and  $\theta_n$  in the expansion of (14). It is noted that (P2) is a single-variable non-convex optimization problem.

Next, we propose a closed-form approximate solution to (P2). The key to approximately solving (P2) in closed-form lies in re-expressing (18) in a more tractable form. In general, any approximation of a nonlinear function can only fit the original function values locally, which we refer to as the trust region. For (P2), the trust region should enclose its optimal solution, denoted by  $\theta_n^*$ .

Define  $f(\theta_n) \triangleq \beta_n^2(\theta_n) \Psi_{n,n} + \beta_n(\theta_n) |\varphi_n| \cos(\arg(\varphi_n) - \theta_n)$ . It is not difficult to observe that for the ideal phase shift model considered in [2]–[4],  $\beta_n(\theta_n)$  and  $\theta_n$  can be designed to maximize  $f(\theta_n)$  (or (18)) by setting  $\beta_n^*(\theta_n) = 1$  and  $\theta_n^* = \arg(\varphi_n), \forall n$ . However, such a reflection design is no longer optimal for a practical IRS due to the dependency of  $\beta_n(\theta_n)$  on  $\theta_n$  as depicted in Fig. 3 (b). For instance, if  $\arg(\varphi_n) = 0$ ,  $\theta_n^* = 0$  may not be a favourable phase design as it yields the lowest reflection amplitude. In this case,  $\theta_n^*$  needs to be properly chosen to balance between  $\beta_n(\theta_n)$  and  $\arg(\varphi_n)$ . In particular, since the minimum  $\beta_n(\theta_n)$  occurs near zero phase shift and approaches the maximum at  $\pi$  and  $-\pi$ ,  $\theta_n^*$  should deviate from  $\arg(\varphi_n)$  towards  $\pi$  (or  $-\pi$ ) when  $\arg(\varphi_n)$  is positive (negative). Based on this, the trust region of the optimal phase shift is presented in the following proposition.

**Algorithm 1** AO-based Algorithm for Solving (P1)

---

```

1: Initialize:  $\{\theta_n\}_{n=1}^N$ .
2: repeat
3:   for  $n = 1$  to  $N$  do
4:     Find  $\theta_n^*$  as the solution to (P2) using (21) with the
       trust region given by (20).
5:   end for
6:   Obtain  $v_n = \beta_n(\theta_n^*)e^{j\theta_n^*}, \forall n$ .
7: until the objective value of (P1) with the obtained  $\mathbf{v}$ 
       reaches convergence.

```

---

*Proposition 2:* The trust region that encloses  $\theta_n^*$  for (P2) is given by

$$\theta_n^* \in [\arg(\varphi_n), (-1)^\lambda \pi], \quad (20)$$

with  $\lambda = 0$  when  $\arg(\varphi_n) \geq 0$  and  $\lambda = 1$  otherwise.  $\blacksquare$

*Proof:* See Appendix B.  $\blacksquare$

Motivated by the above result, a high-quality approximate solution to problem (P2) can be obtained numerically via the one-dimensional (1D) search over  $[\arg(\varphi_n), (-1)^\lambda \pi]$ , which may still be computationally inefficient. Alternatively, a closed-form approximate solution can be obtained by fitting a quadratic function through three points over the trust region (which are obtained via equally sampling the trust region), i.e.,  $\theta_A = \arg(\varphi_n)$ ,  $\theta_B = \frac{\arg(\varphi_n) + (-1)^\lambda \pi}{2}$ , and  $\theta_C = (-1)^\lambda \pi$ , as given in the following proposition.

*Proposition 3:* Let  $f_1 = f(\theta_A)$ ,  $f_2 = f(\theta_B)$ , and  $f_3 = f(\theta_C)$ . The approximate solution to (P2) obtained by fitting a quadratic function through the points  $(\theta_A, f_1)$ ,  $(\theta_B, f_2)$ , and  $(\theta_C, f_3)$  is given by

$$\hat{\theta}_n^* = \frac{\theta_A(f_1 - 4f_2 + 3f_3) + \theta_C(3f_1 - 4f_2 + f_3)}{4(f_1 - 2f_2 + f_3)}. \quad (21)$$

*Proof:* See Appendix C.  $\blacksquare$

It is worth pointing out that Proposition 3 essentially corresponds to a single iteration of the successive quadratic estimation with trust region refinement proposed in [38]. The overall AO-based algorithm to solve (P1) is given in Algorithm 1.

#### D. Penalty-based Algorithm

To deal with the non-convex constraints in (15), we next resort to a penalty-based method that penalizes the constraint violation by adding a constraint-related penalty term to the objective function of (P1). To this end, the penalized version of (P1) is formulated as

$$(P3) : \max_{\mathbf{v}, \{\theta_n\}} \|\mathbf{v}^H \Phi + \mathbf{h}_d^H\|^2 - \mu \sum_{n=1}^N |v_n - \beta_n(\theta_n)e^{j\theta_n}|^2 \quad (22)$$

$$\text{s.t. } -\pi \leq \theta_n \leq \pi, n = 1, \dots, N, \quad (23)$$

where  $\mu > 0$  is the penalty parameter that imposes a cost for the constraint violation of the constraints in (15). In particular, when  $\mu \rightarrow \infty$ , solving the above problem yields an approximate solution to (P1) [39]. However, initializing

$\mu$  to be a sufficiently small value generally yields a good starting point for the proposed algorithm, even though this point may be infeasible for (P1). By gradually increasing the value of  $\mu$  by a factor of  $\varrho > 1$ , we can maximize the original objective function, i.e.,  $\|\mathbf{v}^H \Phi + \mathbf{h}_d^H\|^2$ , and obtain a solution that satisfies all the equality constraints in (15) within a predefined accuracy. This thus leads to a two-layer iterative algorithm, where the inner layer solves the penalized optimization problem (P3) while the outer layer updates the penalty coefficient  $\mu$ , until the convergence is achieved.

For any given  $\mu > 0$ , (P3) is still a non-convex optimization problem due to the non-convex objective function. However, it is observed from (22) that  $\mathbf{v}$  can be updated with fixed  $\{\theta_n\}_{n=1}^N$ , and  $\{\theta_n\}_{n=1}^N$  can be updated in parallel with fixed  $\mathbf{v}$ , which thus motivates us to apply the block coordinate descent (BCD) method to solve (P3) efficiently. The convergence is achieved when the fractional increase of (22) is below a positive yet sufficiently small threshold and the details are given as follows.

1) For any given  $\{\theta_n\}_{n=1}^N$ ,  $\mathbf{v}$  in (P3) can be optimized by solving the following problem

$$(P3.1) : \max_{\mathbf{v}} \|\mathbf{v}^H \Phi + \mathbf{h}_d^H\|^2 - \mu \|\mathbf{v} - \mathbf{a}\|^2, \quad (24)$$

where  $\mathbf{a} = [\beta_1(\theta_1)e^{j\theta_1}, \dots, \beta_N(\theta_N)e^{j\theta_N}]^T$ . It is not difficult to observe that (P3.1) is an unconstrained non-convex optimization problem due to the first and second terms of (24) being respectively convex and concave, for which we can apply the concave-convex procedure (CCCP) [40] to approximately solve it in an iterative manner. Specifically, at each iteration  $l = 1, 2, \dots$ , we approximate the first term of the objective function in (P3.1) by a linear function using its first-order Taylor series at a given point  $\mathbf{v}^{(l)}$  to form a convex approximate optimization problem, which is given by (with constant terms ignored)

$$(P3.2) : \max_{\mathbf{v}} 2(\Phi \Phi^H \mathbf{v}^{(l)} + \Phi \mathbf{h}_d)^H (\mathbf{v} - \mathbf{v}^{(l)}) - \mu \|\mathbf{v} - \mathbf{a}\|^2. \quad (25)$$

Next, we set the value of  $\mathbf{v}$  for iteration  $l+1$  as the optimal solution to (P3.2) at iteration  $l$ , and the algorithm continues until the objective value of (P3.1) reaches convergence. It is not difficult to observe that (P3.2) is an unconstrained convex optimization problem, for which the optimal solution in closed-form can be easily obtained as (by setting the first-order derivative of the objective function with respect to  $\mathbf{v}$  equal to zero)

$$\mathbf{v}^{(l+1)} = \frac{\Phi \Phi^H \mathbf{v}^{(l)} + \Phi \mathbf{h}_d + \mu \mathbf{a}}{\mu}. \quad (26)$$

2) For any given  $\mathbf{v}$ ,  $\{\theta_n\}_{n=1}^N$  in (P3) can be optimized by solving the following problem

$$(P3.3) : \max_{\{\theta_n\}} - \sum_{n=1}^N |v_n - \beta_n(\theta_n)e^{j\theta_n}|^2 \quad (27)$$

$$\text{s.t. } -\pi \leq \theta_n \leq \pi, n = 1, \dots, N. \quad (28)$$

It is noted that this is a non-convex optimization problem due to the fact that  $\beta_n(\theta_n)$  is non-convex in  $\theta_n$ . However, since

**Algorithm 2** Penalty-based Algorithm for Solving (P1)

- 1: **Initialize:**  $\{\theta_n\}_{n=1}^N$  and  $\mu > 0$ .
- 2: **repeat**
- 3:   **repeat**
- 4:     Update  $\mathbf{v}$  as the solution to (P3.1).
- 5:     Update  $\{\theta_n\}_{n=1}^N$  using (21) with the trust region given by (31).
- 6:   **until** The fractional increase of the objective value of (P3) is below a threshold  $\epsilon_1 > 0$  or the maximum number of iterations is reached.
- 7:   Update the penalty coefficient  $\mu \leftarrow \varrho\mu$ .
- 8: **until** The constraint violation ( $\sum_{n=1}^N |v_n - \beta_n(\theta_n)e^{j\theta_n}|^2$ ) is below a threshold  $\epsilon_2 > 0$ .

$\theta_n$ 's are fully separable in the objective function, solutions to  $\{\theta_n\}_{n=1}^N$  can be obtained by solving  $N$  independent subproblems in parallel. By expanding  $|v_n - \beta_n(\theta_n)e^{j\theta_n}|^2$  and ignoring constant terms, each corresponding subproblem is given by

$$(P3.4) : \max_{\theta_n} 2\beta_n(\theta_n)|v_n| \cos(\psi_n - \theta_n) - \beta_n^2(\theta_n) \quad (29)$$

$$\text{s.t. } -\pi \leq \theta_n \leq \pi. \quad (30)$$

where  $\psi_n = \arg(v_n)$ .

In contrast to (P2), the trust region given in Proposition 2 is not applicable for (P3.4) due to the negative term in its objective function, i.e.,  $-\beta_n^2(\theta_n)$ . Nevertheless, it can be observed from (29) that its  $\cos(\cdot)$  term is maximized when  $\theta_n = \psi_n$  and the whole function is maximized when  $\theta_n$  slightly deviates away from  $\psi_n$  based on  $v_n$ . The trust region is thus formally presented in the following proposition.

*Proposition 4:* The trust region that encloses the optimal solution of (P3.4), denoted by  $\theta_n^*$ , is given by

$$\theta_n^* \in \begin{cases} [\psi_n, \psi_n + (-1)^\lambda \Delta] & \text{if } \frac{\beta_n(\psi_n) + \beta_n(\psi_n + \Delta)}{2} < |v_n|, \\ [\psi_n, \psi_n - (-1)^\lambda \Delta] & \text{if } \frac{\beta_n(\psi_n) + \beta_n(\psi_n - \Delta)}{2} > |v_n|, \end{cases} \quad (31)$$

where  $\Delta \geq 0$ , and  $\lambda = 0$  when  $\psi_n \geq 0$  and  $\lambda = 1$  otherwise.

*Proof:* See Appendix D. ■

By choosing a proper value for  $\Delta$  and fitting a quadratic function through three points over the trust region (which are obtained via equally sampling the trust region), a closed-form approximate solution to (P3.4) can be similarly obtained as Proposition 3. The overall penalty-based algorithm to solve (P1) is given in Algorithm 2.

## V. MULTIUSER BEAMFORMING OPTIMIZATION

In this section, we consider the general multiuser setup. Specifically, we propose two efficient algorithms to solve the multiuser beamforming optimization problem suboptimally, by extending the solutions for the single-user case.

### A. Problem Formulation

We aim to minimize the total transmit power at the AP by jointly optimizing the transmit beamforming at the AP and reflect beamforming at the IRS, subject to the individual SINR

constraints at all users. Accordingly, the problem is formulated as

$$(P4) : \min_{\{\mathbf{w}_k\}, \mathbf{v}, \{\theta_n\}} \sum_{k=1}^K \|\mathbf{w}_k\|^2 \quad (32)$$

$$\text{s.t. } \frac{|(\mathbf{v}^H \Phi_k + \mathbf{h}_{d,k}^H) \mathbf{w}_k|^2}{\sum_{j \neq k}^K |(\mathbf{v}^H \Phi_k + \mathbf{h}_{d,k}^H) \mathbf{w}_j|^2 + \sigma_k^2} \geq \gamma_k, \forall k, \quad (33)$$

$$v_n = \beta_n(\theta_n) e^{j\theta_n}, n = 1, \dots, N, \quad (34)$$

$$-\pi \leq \theta_n \leq \pi, n = 1, \dots, N, \quad (35)$$

where  $\gamma_k > 0$  is the minimum SINR requirement of user  $k$ . Note that (P4) is a non-convex optimization problem due to the coupling between  $\mathbf{w}_k$ 's and  $\mathbf{v}$  in (33) and non-convex constraints in (34), for which we propose two efficient algorithms by generalizing the two approaches in the single-user case.

### B. Extended Penalty-based Algorithm

First, we introduce new auxiliary variables to decouple  $\mathbf{w}_k$ 's and  $\mathbf{v}$  in (33). To this end, let  $\mathbf{h}_k^H \mathbf{w}_j = x_{k,j}$  with  $\mathbf{h}_k^H = \mathbf{v}^H \Phi_k + \mathbf{h}_{d,k}^H$ ,  $k, j = 1, \dots, K$ . Then the SINR constraints can be expressed as

$$\frac{|x_{k,k}|^2}{\sum_{j \neq k}^K |x_{k,j}|^2 + \sigma_k^2} \geq \gamma_k, k = 1, \dots, K. \quad (36)$$

By replacing (33) with (36), (P4) is equivalently transformed to

$$(P5) : \min_{\{\mathbf{w}_k\}, \mathbf{v}, \{\theta_n\}, \{x_{k,j}\}} \sum_{k=1}^K \|\mathbf{w}_k\|^2 \quad (37)$$

$$\text{s.t. } \frac{|x_{k,k}|^2}{\sum_{j \neq k}^K |x_{k,j}|^2 + \sigma_k^2} \geq \gamma_k, \forall k, \quad (38)$$

$$v_n = \beta_n(\theta_n) e^{j\theta_n}, n = 1, \dots, N, \quad (39)$$

$$\mathbf{h}_k^H \mathbf{w}_j = x_{k,j}, k, j = 1, \dots, K, \quad (40)$$

$$-\pi \leq \theta_n \leq \pi, n = 1, \dots, N. \quad (41)$$

(P5) is still non-convex and difficult to be optimally solved in general due to the non-convex constraints in (39) and the coupling between  $\mathbf{w}_k$ 's and  $\mathbf{v}$  is still present with the newly added equality constraint in (40). To overcome such difficulty, we resort to the penalty-based method by adding equality constraint-related penalty terms to the objective function of (P5), yielding the following optimization problem

$$(P6) : \min_{\{\mathbf{w}_k\}, \mathbf{v}, \{\theta_n\}, \{x_{k,j}\}} \sum_{k=1}^K \|\mathbf{w}_k\|^2 + \mu \sum_{n=1}^N |v_n - \beta_n(\theta_n)e^{j\theta_n}|^2 + \nu \sum_{k=1}^K \sum_{j=1}^K |\mathbf{h}_k^H \mathbf{w}_j - x_{k,j}|^2 \quad (42)$$

$$\text{s.t. } \frac{|x_{k,k}|^2}{\sum_{j \neq k}^K |x_{k,j}|^2 + \sigma_k^2} \geq \gamma_k, \forall k, \quad (43)$$

$$-\pi \leq \theta_n \leq \pi, n = 1, \dots, N, \quad (44)$$

where  $\mu > 0$  and  $\nu > 0$  denote the penalty coefficients used for penalizing the violation of equality constraints in (P5).

Similarly to problem (P3), we propose a two-layer iterative algorithm. Specifically, the inner layer solves the penalized optimization problem (P6) by applying the BCD method while the outer layer updates  $\mu$  and  $\nu$ , until the convergence is achieved. To this end, the entire optimization variables in (P6) are partitioned into four blocks, i.e.,  $\{\mathbf{w}_k\}_{k=1}^K$ ,  $\mathbf{v}$ ,  $\{\theta_n\}_{n=1}^N$ , and  $\{x_{k,j}\}_{k,j=1}^K$ . Then, we can minimize (P6) by alternately optimizing each of the above four blocks in one iteration with the other three blocks fixed, and iterating the above until the convergence is reached, which is detailed as follows.

1) For any given  $\mathbf{v}$ ,  $\{\theta_n\}_{n=1}^N$  and  $\{x_{k,j}\}_{k,j=1}^K$ ,  $\{\mathbf{w}_k\}_{k=1}^K$  can be optimized by solving the following problem

$$(P6.1) : \min_{\{\mathbf{w}_k\}} \sum_{k=1}^K \|\mathbf{w}_k\|^2 + \nu \sum_{k=1}^K \sum_{j=1}^K |\mathbf{h}_k^H \mathbf{w}_j - x_{k,j}|^2. \quad (45)$$

It is not difficult to observe that (P6.1) is an unconstrained convex optimization problem, for which the optimal solution in closed-form can be easily obtained by setting the first-order derivative of the objective function with respect to  $\mathbf{w}_k$  equal to zero, and is given by

$$\mathbf{w}_k^* = \nu \left( \mathbf{I}_M + \nu \sum_{j=1}^K \mathbf{h}_k \mathbf{h}_k^H \right)^{-1} \left( \sum_{j=1}^K \mathbf{h}_j x_{j,k} \right). \quad (46)$$

It is worth pointing out that all  $\mathbf{w}_k^*$ 's for different users can be updated in parallel by using (46).

2) For any given  $\{\mathbf{w}_k\}_{k=1}^K$ ,  $\{\theta_n\}_{n=1}^N$  and  $\{x_{k,j}\}_{k,j=1}^K$ ,  $\mathbf{v}$  can be optimized by solving the following problem

$$(P6.2) : \min_{\mathbf{v}} \mu \|\mathbf{v} - \mathbf{a}\|^2 + \nu \sum_{k=1}^K \sum_{j=1}^K |\mathbf{h}_k^H \mathbf{w}_j - x_{k,j}|^2, \quad (47)$$

where  $\mathbf{a} = [\beta_1(\theta_1)e^{j\theta_1}, \dots, \beta_N(\theta_N)e^{j\theta_N}]^T$ . By applying the change of variables,  $\text{diag}(\mathbf{h}_{r,k}^H) \mathbf{G} \mathbf{w}_j = \bar{\mathbf{d}}_{k,j}$  and  $-\mathbf{h}_{d,k}^H \mathbf{w}_j + x_{k,j} = \bar{C}_{k,j}$ , we have

$$\begin{aligned} \mathbf{h}_k^H \mathbf{w}_j - x_{k,j} &= \mathbf{v}^H \text{diag}(\mathbf{h}_{r,k}^H) \mathbf{G} \mathbf{w}_j + \mathbf{h}_{d,k}^H \mathbf{w}_j - x_{k,j} \\ &= \mathbf{v}^H \bar{\mathbf{d}}_{k,j} - \bar{C}_{k,j}. \end{aligned} \quad (48)$$

Problem (P6.2) is thus equivalent to

$$(P6.2 - \text{EQ}) : \min_{\mathbf{v}} \mu \|\mathbf{v} - \mathbf{a}\|^2 + \nu \sum_{k=1}^K \sum_{j=1}^K |\mathbf{v}^H \bar{\mathbf{d}}_{k,j} - \bar{C}_{k,j}|^2, \quad (49)$$

for which the optimal solution in closed-form can be similarly obtained by setting the first-order derivative of the objective function with respect to  $\mathbf{v}$  equal to zero, and is given by

$$\begin{aligned} \mathbf{v}^* &= \left( \mu \mathbf{I}_N + \nu \sum_{k=1}^K \sum_{j=1}^K \bar{\mathbf{d}}_{k,j} \bar{\mathbf{d}}_{k,j}^H \right)^{-1} \\ &\quad \times \left( \mu \mathbf{a} + \nu \sum_{k=1}^K \sum_{j=1}^K \bar{\mathbf{d}}_{k,j} \bar{C}_{k,j}^H \right). \end{aligned} \quad (50)$$

3) For any given  $\{\mathbf{w}_k\}_{k=1}^K$ ,  $\mathbf{v}$  and  $\{x_{k,j}\}_{k,j=1}^K$ ,  $\{\theta_n\}_{n=1}^N$  can be optimized by solving the following problem

$$(P6.3) : \min_{\{\theta_n\}} \sum_{n=1}^N |v_n - \beta_n(\theta_n)e^{j\theta_n}|^2, \quad (51)$$

which is essentially identical to (P3.3) and thus can be similarly solved (i.e., by parallelly solving  $N$  independent subproblems in closed-form) according to Proposition 3, while the trust region is given by Proposition 4.

4) For any given  $\{\mathbf{w}_k\}_{k=1}^K$ ,  $\mathbf{v}$  and  $\{\theta_n\}_{n=1}^N$ ,  $\{x_{k,j}\}_{k,j=1}^K$  can be optimized by solving the following problem

$$(P6.4) : \min_{\{x_{k,j}\}} \sum_{k=1}^K \sum_{j=1}^K |\mathbf{h}_k^H \mathbf{w}_j - x_{k,j}|^2 \quad (52)$$

$$\text{s.t. } \frac{|x_{k,k}|^2}{\sum_{j \neq k}^K |x_{k,j}|^2 + \sigma_k^2} \geq \gamma_k, \forall k. \quad (53)$$

It is not difficult to observe that the optimization variables with respect to different users are separable in both the objective function and constraints. As a result, we can solve (P6.4) by solving  $K$  independent subproblems in parallel, each with only one single SINR constraint. To this end, the corresponding subproblem for the  $k$ -th user with respect to  $x_{k,j}$ 's,  $\forall j = 1, \dots, K$ , can be given by

$$(P6.5) : \min_{\{x_{k,j}, \forall j\}} \sum_{j=1}^K |\mathbf{h}_k^H \mathbf{w}_j - x_{k,j}|^2 \quad (54)$$

$$\text{s.t. } \frac{|x_{k,k}|^2}{\sum_{j \neq k}^K |x_{k,j}|^2 + \sigma_k^2} \geq \gamma_k. \quad (55)$$

Although (P6.5) is non-convex, it has been shown in [18] that this problem can be efficiently and optimally solved by applying the Lagrange duality method. Specifically, by exploiting the first-order optimality condition, the optimal solution is given by

$$x_{k,k}^* = \frac{\mathbf{h}_k^H \mathbf{w}_k}{1 - \lambda_k}, \quad (56)$$

$$x_{k,j}^* = \frac{\mathbf{h}_k^H \mathbf{w}_j}{1 + \lambda_k \gamma_k}, j \neq k, k = 1, \dots, K, \quad (57)$$

where  $\lambda_k$  is the dual variable. If the SINR constraint in (55) is not met with equality at the optimal solution, then  $\lambda_k = 0$ . Otherwise, the optimal dual variable can be efficiently obtained by substituting (56)-(57) into (55), i.e.,  $\frac{|\mathbf{h}_k^H \mathbf{w}_k|^2}{(1 - \lambda_k)^2} - \sum_{j \neq k}^K \frac{\gamma_k |\mathbf{h}_k^H \mathbf{w}_j|^2}{(1 + \lambda_k \gamma_k)^2} - \gamma_k \sigma_k^2 = 0$ , and performing a simple bisection search over  $0 \leq \lambda_k < 1$ .

The overall penalty-based algorithm to solve (P4) is given in Algorithm 3. It should be noted that Algorithm 3 is computationally efficient as the optimization variables in steps 4, 5, and 6 can be updated in parallel by using closed-form expressions, and those in step 6 can be obtained by using the simple bisection search. In particular, it can be shown that the complexity of solving (P6.1) is  $\mathcal{O}(K(N^2 + NM + M^2) + M^3)$ , that of solving (P6.2) is  $\mathcal{O}(K^2(N^2 + NM + M^2) + N^3)$ , that of solving (P6.3) is  $\mathcal{O}(1)$ , and that of solving (P6.4) is  $\mathcal{O}(K^2 \log_2(1/\epsilon_3))$  where  $\epsilon_3$  denotes the accuracy for the bisection search. Thus, the overall complexity of Algorithm 3 is given by  $\mathcal{O}(I_{\text{inn}} I_{\text{out}}(N^3 + M^3 + K^2(N^2 + NM + M^2) + K^2 \log_2(1/\epsilon_3)))$  where  $I_{\text{inn}}$  and  $I_{\text{out}}$  respectively denote the inner and outer iteration numbers required for convergence.

### Algorithm 3 Extended Penalty-based Algorithm

- 1: **Initialize:**  $\mathbf{v}$ ,  $\{\theta_n\}_{n=1}^N$ ,  $\{x_{k,j}\}_{k,j=1}^K$ ,  $\mu > 0$ , and  $\nu > 0$
- 2: **repeat**
- 3:   **repeat**
- 4:     Update  $\{\mathbf{w}_k\}_{k=1}^K$  by solving (P6.1).
- 5:     Update  $\mathbf{v}$  by solving (P6.2).
- 6:     Update  $\{\theta_n\}_{n=1}^N$  by solving (P6.3).
- 7:     Update  $\{x_{k,j}\}_{k,j=1}^K$  by solving (P6.4).
- 8:   **until** The fractional decrease of the objective value of (P6) is below a threshold  $\epsilon_1 > 0$  or the maximum number of iterations is reached.
- 9:   Update the penalty coefficients as  $\mu \leftarrow \varrho\mu$  and  $\nu \leftarrow \varrho\nu$ .
- 10: **until** The constraint violation is below a threshold  $\epsilon_2 > 0$  or  $\sum_{k=1}^K \|\mathbf{w}_k\|^2$  reaches convergence.

### C. Two-Stage Algorithm

Inspired by the combined channel power gain maximization problem (P1) for the single-user case, we next propose a two-stage algorithm with lower complexity as compared to the penalty-based algorithm. Specifically, the phase shifts at the IRS are optimized in the first stage by solving the following weighted effective channel power gain maximization problem.

$$(P7.1) : \max_{\mathbf{v}, \{\theta_n\}} \sum_{k=1}^K \Psi_k \|(\mathbf{v}^H \Phi_k + \mathbf{h}_{d,k}^H)\|^2 \quad (58)$$

$$\text{s.t. } v_n = \beta_n(\theta_n) e^{j\theta_n}, n = 1, \dots, N, \quad (59)$$

$$-\pi \leq \theta_n \leq \pi, n = 1, \dots, N, \quad (60)$$

where we set the weights to be  $\Psi_k = \frac{1}{\gamma_k \sigma_k^2}, k = 1, \dots, K$ , motivated by the constraint in (33). This aims to align the phases of different user channels so as to maximize the active and passive beamforming gains of the system. (P7.1) can be similarly solved by adopting the penalty-based technique proposed in Section IV, thus the details are omitted for brevity.

In the second stage, we solve the following problem to obtain the optimal transmit beamforming with the phase shifts obtained from (P7.1),

$$(P7.2) : \min_{\{\mathbf{w}_k\}} \sum_{k=1}^K \|\mathbf{w}_k\|^2 \quad (61)$$

$$\text{s.t. } \frac{|\mathbf{h}_k^H \mathbf{w}_k|^2}{\sum_{j \neq k} |\mathbf{h}_j^H \mathbf{w}_j|^2 + \sigma_k^2} \geq \gamma_k, \forall k, \quad (62)$$

where  $\mathbf{h}_k^H = \mathbf{v}^H \Phi_k + \mathbf{h}_{d,k}^H$ . Note that (P7.2) is the conventional power minimization problem in the multiuser MISO downlink broadcast channel, where its optimal solution known as the minimum mean squared error (MMSE) based linear precoder can be obtained by using, e.g., a fixed-point iteration algorithm based on the uplink-downlink duality [2], [41], [42], i.e.,

$$\mathbf{w}_k^* = \sqrt{p_k} \hat{\mathbf{w}}_k^*, \quad (63)$$

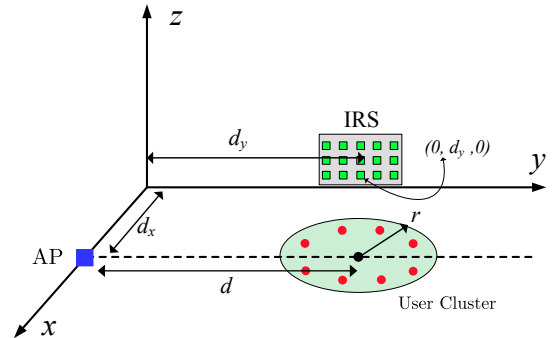


Fig. 5: Simulation setup.

where

$$\begin{bmatrix} p_1 \\ \vdots \\ p_K \end{bmatrix} = \mathbf{Q}^{-1} \begin{bmatrix} \sigma_1^2 \\ \vdots \\ \sigma_K^2 \end{bmatrix}, \quad (64)$$

$$\mathbf{Q}(i, j) = \begin{cases} \frac{1}{\gamma_i} |\mathbf{h}_i^H \hat{\mathbf{w}}_i^*|^2, & i = j, \\ -|\mathbf{h}_i^H \hat{\mathbf{w}}_j^*|^2, & i \neq j, \forall i, j \in \{1, \dots, K\}, \end{cases} \quad (65)$$

$$\hat{\mathbf{w}}_k^* = \frac{(\mathbf{I}_M + \sum_{i=1}^K \frac{\rho_i}{\sigma_i^2} \mathbf{h}_i \mathbf{h}_i^H)^{-1} \mathbf{h}_k}{\|(\mathbf{I}_M + \sum_{i=1}^K \frac{\rho_i}{\sigma_i^2} \mathbf{h}_i \mathbf{h}_i^H)^{-1} \mathbf{h}_k\|}, \quad (66)$$

$$\rho_k = \frac{\sigma_k^2}{(1 + \frac{1}{\gamma_k}) \mathbf{h}_k^H (\mathbf{I}_M + \sum_{i=1}^K \frac{\rho_i}{\sigma_i^2} \mathbf{h}_i \mathbf{h}_i^H)^{-1} \mathbf{h}_k}, \forall k. \quad (67)$$

Specifically,  $\rho_k$ 's can be obtained by using the fixed-point algorithm to solve  $K$  equations in (67). With  $\rho_k$ 's,  $\hat{\mathbf{w}}_k^*$ 's can be obtained from (66) and then  $p_k$ 's can be obtained from (64). Finally,  $\mathbf{w}_k^*$ 's are obtained by using (63) with  $\hat{\mathbf{w}}_k^*$ 's and  $p_k$ 's.

The overall complexity of the two-stage algorithm can be shown to be  $\mathcal{O}(I_{itr}(KM^2 + M^3) + K^3 + K^2M + KMN + I_{inn}I_{out}(N^3 + KN^2))$  where  $I_{itr}$  denotes the number of iterations required for obtaining  $\rho_k$ 's in (67), and  $I_{inn}$ ,  $I_{out}$  respectively denote the inner and outer iteration numbers required for the convergence of (P7.1). Compared to the extended penalty-based algorithm proposed in Section V-B, the two-stage algorithm has lower computational complexity as (P7.1) and (P7.2) only need to be respectively solved for one time.

## VI. SIMULATION RESULTS

In this section, numerical results are provided to evaluate the performance of the proposed algorithms. We consider a system that operates on a carrier frequency of 2.4 GHz, which corresponds to the signal attenuation at a reference distance of 1 m about 40 dB. A three-dimensional (3D) coordinate system is considered as shown in Fig. 5, where a uniform linear array (ULA) at the AP and a uniform rectangular array (URA) at the IRS are located in  $x$ -axis and  $y$ - $z$  plane, respectively. The reference antenna/element at the AP/IRS are respectively located at  $(d_x, 0, 0)$  and  $(0, d_y, 0)$ , where in both cases a half-wavelength (i.e., 6.25 centimeter) spacing is assumed among

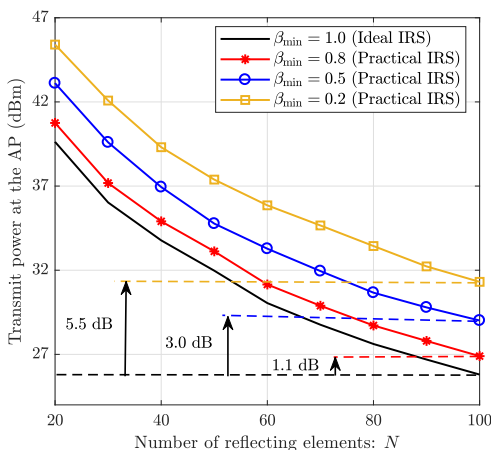


Fig. 6: AP transmit power versus number of reflecting elements.

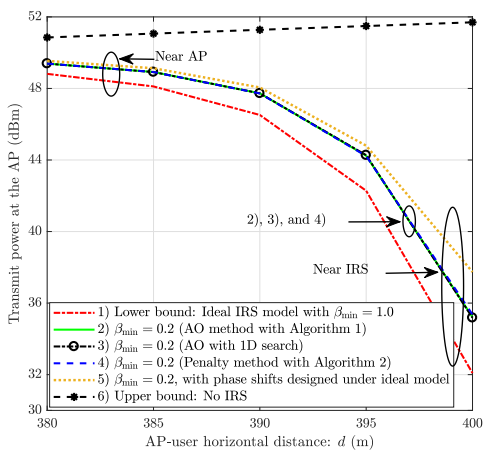


Fig. 7: AP transmit power versus the AP-user horizontal distance.

adjacent antennas/elements. For the IRS, we set  $N = N_y N_z$  where  $N_y$  and  $N_z$  denote the number of reflecting elements along  $y$ -axis and  $z$ -axis, respectively. For the purpose of exposition, we fix  $N_y = 5$  and increase  $N_z$  linearly with  $N$ . The  $K$  users are uniformly and randomly distributed in a cluster, which is centered at  $(d_x, d, 0)$  with radius  $r$ . Rayleigh fading is assumed for all the channels involved. The path loss exponents are set to 2.2, 2.8, and 3.8 for the channels between AP-IRS, IRS-user, and AP-user, respectively, as IRSs are usually deployed for users with weak AP-user channels and their locations can be properly selected to avoid severe blockage with the AP. Moreover, we set  $\sigma_k^2 = -94$  dBm,  $\forall k$ . The phase shift model parameters are set as follows unless specified otherwise:  $\beta_{\min} = 0.2$ ,  $\alpha = 1.6$ , and  $\phi = 0.43\pi$  according to [32].

#### A. Single-User Case

We first consider a single-user system with the SNR target  $\gamma = 10$  dB and  $M = 4$ . The user is assumed to lie in the cluster center, denoted by  $(d_x, d, 0)$  with  $d_x = 2$  m. Moreover, it is assumed that  $d_y = 400$  m.

To validate the theoretical analysis in Proposition 1, we plot in Fig. 6 the AP transmit power versus the number of

reflecting elements  $N$  when  $d = 400$  m. In particular, IRS phase shifts are obtained for the ideal IRS (i.e.,  $\beta_{\min} = 1$ ) by using Algorithm 1 and the obtained phase shifts are then applied to the practical IRS with  $\beta_{\min} = 0.8$ ,  $\beta_{\min} = 0.5$ , or  $\beta_{\min} = 0.2$ . Since the power loss is not sensitive to parameter  $\alpha$  in the phase shift model, we fix  $\alpha = 1.6$  in simulations. From Fig. 6, it is observed that as  $N$  increases, the performance gap between the ideal case ( $\beta_{\min} = 1$ ) and practical cases ( $\beta_{\min} = 0.8$ ,  $\beta_{\min} = 0.5$ , and  $\beta_{\min} = 0.2$ ) first increases and then approaches a constant that is determined by  $\eta(\beta_{\min}, \alpha)$  given in (17) and has also been shown in Table I. This is due to the fact that when  $N$  is moderate, the signal power of the AP-user link is comparable to that of the IRS-user link, thus the power loss due to the IRS hardware imperfection is more pronounced with increasing  $N$ . However, when  $N$  is sufficiently large such that the reflected signal power by the IRS dominates in the total receive power at the user, the power loss arising from the imperfect IRS reflection converges to that in accordance with the asymptotic analysis given in Proposition 1.

Next, by varying  $d$ , the required AP transmit power is compared in Fig. 7 for the following schemes with  $N = 40$ :

- 1) Lower bound: solve (P1) with  $\beta_{\min} = 1$  (i.e., ideal IRS) by using semidefinite relaxation (SDR) with Gaussian randomization which has been shown to achieve near-optimal performance in [2].
- 2) AO method (Algorithm 1): solve (P2) with  $\beta_{\min} = 0.2$  (i.e., practical IRS) by using Proposition 3 with the trust region given by Proposition 2.
- 3) AO method (exhaustive search): solve (P2) with  $\beta_{\min} = 0.2$  by using the 1D search.
- 4) Penalty-based method (Algorithm 2): solve (P3) with  $\beta_{\min} = 0.2$ . We set  $\epsilon_1 = 10^{-3}$ ,  $\epsilon_2 = 10^{-8}$ ,  $\varrho = 1.3$ ,  $\mu^{(1)} = 10^{-15}$ , and  $\Delta = 0.05$ .
- 5) Ideal IRS assumption: the phase shifts designed for the IRS with  $\beta_{\min} = 1$  are applied to the practical IRS with  $\beta_{\min} = 0.2$ .
- 6) Upper bound: the system without using the IRS by setting  $\mathbf{w}^* = \sqrt{P} \frac{\mathbf{h}_d}{\|\mathbf{h}_d\|}$  with  $P^* = \frac{\gamma \sigma^2}{\|\mathbf{h}_d\|^2}$ .

Note that the initial phase shift values of the proposed penalty-based and AO algorithms, i.e.,  $\{\theta_n\}_{n=1}^N$ , are randomly selected from  $\{\pi, -\pi\}$  such that each reflecting element has the maximum reflection amplitude. Moreover,  $\mu^{(1)}$  is chosen such that  $\|\mathbf{v}^H \Phi + \mathbf{h}_d^H\|^2 \gg \mu^{(1)} \sum_{n=1}^N |v_n - \beta_n(\theta_n)| e^{j\theta_n}|^2$ .

It is observed from Fig. 7 that scheme 1) has the best performance. This is due to the fact that when each of the reflecting elements in the ideal phase shift model has the unity reflection amplitude (the maximum value) regardless of its phase shift, IRS reflection can be designed to achieve the maximal phase alignment between the IRS-reflected and non-IRS-reflected signals at the receiver without causing any performance degradation. In contrast, a substantial power loss is incurred under scheme 5) as the designed phase shifts in this case only achieve the maximal phase alignment at the receiver, but result in a much lower reflection amplitude (near  $\beta_{\min}$ ) at certain reflecting elements depending on their phase shifts. However, schemes 2), 3), and 4) (our proposed algorithms)

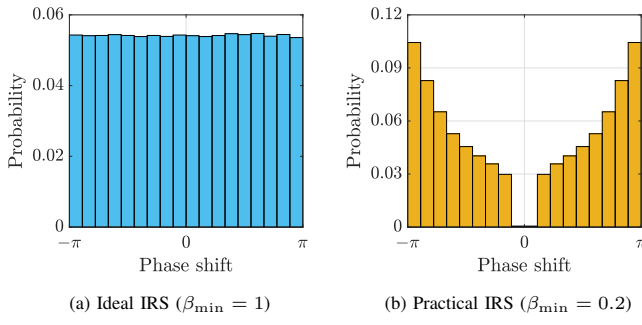


Fig. 8: Distribution of IRS phase shift values over reflecting elements.

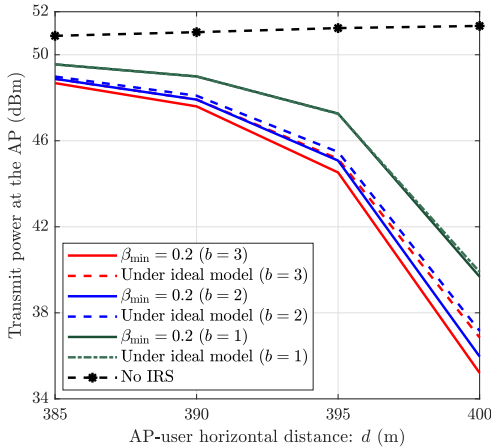


Fig. 9: Achievable rate versus  $d$  in the case of discrete phase shift.

significantly outperform scheme 5) thanks to their ability to strike a balance between the reflected signal amplitude by individual elements and phase alignment over all the elements so as to achieve the maximum signal power at the receiver. Moreover, schemes 2), 3), and 4) perform very close to each other. This suggests that AO and penalty-based algorithms with Proposition 3 provide a practically appealing solution to (P1) considering their low complexity. It is also observed that when the user moves closer to the IRS, the performance gap between the proposed schemes and scheme 5) increases. This is due to the fact that the user benefits from the stronger reflecting channel via IRS ( $\mathbf{h}_r$ ), and therefore proper reflection design based on the practical IRS model becomes more crucial. In contrast, when the user moves toward the AP, the above performance gap decreases as the AP-user direct channel ( $\mathbf{h}_d$ ) becomes dominant, thus reducing the effectiveness of the IRS reflection.

Next, in Fig. 8, we plot the phase shift distribution over the IRS reflecting elements. In particular, we solve (P1) by using Algorithm 1 for the ideal IRS with  $\beta_{\min} = 1$  and the practical IRS with  $\beta_{\min} = 0.2$  to empirically obtain the phase shift distribution. It is observed from Fig. 8(a) that when  $\beta_{\min} = 1$ , the phase shift value is uniformly distributed in  $[-\pi, \pi]$ . However, when  $\beta_{\min} = 0.2$ , the probability increases from zero to  $\pi$  or  $-\pi$  while there is nearly zero probability near the zero phase shift, as shown in Fig. 8(b). This is expected since the minimum reflection amplitude (i.e.,  $\beta_{\min}$ ) occurs at zero phase shift and asymptotically approaches the maximum

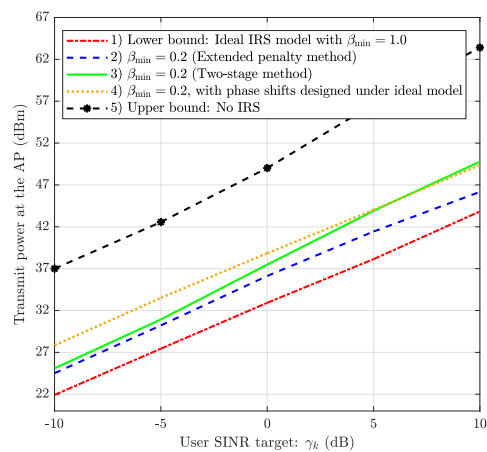


Fig. 10: AP transmit power versus user SINR target.

of one at  $\pi$  or  $-\pi$ , thus the optimized phase shift is more concentrated towards either  $\pi$  or  $-\pi$  to maximize the effective channel power gain.

In practice, it is difficult to implement continuous phase shifts at each of the reflecting elements [43]. To take this into account, we consider the practical setup where the phase shift at each element of the IRS can only take a finite number of discrete values, which are assumed to be equally spaced in  $[-\pi, \pi]$ . Denote by  $b$  the number of bits used to represent each of the levels. Then the set of phase shifts at each element is given by  $\mathcal{F} = \{0, \Delta\theta, \dots, \Delta\theta(U-1)\}$  where  $\Delta\theta = 2\pi/U$  and  $U = 2^b$ . In Fig. 9, we compare the AP transmit power for different values of  $b$  when the user moves closer to the IRS with  $\beta_{\min} = 0.2$  and  $N = 40$ . By solving (P2) with 1D search over  $\mathcal{F}$ , we compare the performance of the following two schemes for designing the discrete IRS phase shifts: i) based on the actual value of  $\beta_{\min}$  (i.e., 0.2); and ii) based on the ideal model (i.e., assuming  $\beta_{\min} = 1$ ). It is observed that for  $b = 1$ , both schemes have nearly the same performance and thus the consideration of IRS hardware imperfection is not necessary. However, when  $b$  increases, the performance gap between these two schemes increases. This is expected as  $b$  increases, the reflected signal power by the IRS is more dominant in the total receive power at the user, thus the performance loss due to the inaccurate (ideal) phase shift model becomes more pronounced.

### B. Multiuser Case

Next, we consider a multiuser system with  $K = 4$ ,  $M = 4$ ,  $N = 40$ ,  $d_x = 3.5$  m,  $d_y = 400$  m, and  $r = 2.5$  m. Without loss of generality, we assume that all users have the same SINR target, i.e.,  $\gamma_k = \gamma, \forall k$ . We set  $\epsilon_1 = 10^{-3}$ ,  $\epsilon_2 = 10^{-5}$ ,  $\varrho = 1.3$ ,  $\mu^{(1)} = 10^{-14}$ ,  $\nu^{(1)} = 10$ , and  $\Delta = 0.05$ . Note that  $\mu^{(1)}$  and  $\nu^{(1)}$  are chosen such that  $\sum_{k=1}^K \|\mathbf{w}_k\|^2 \gg \mu^{(1)} \sum_{n=1}^N |v_n - \beta_n(\theta_n)|^2 + \nu^{(1)} \sum_{k=1}^K \sum_{j=1}^K |\mathbf{h}_k^H \mathbf{w}_j - x_{k,j}|^2$ . Other system parameters are the same as in Section VI-A (if not specified otherwise).

By fixing  $d = 400$  m and varying the SINR target, in Fig. 10, we plot the required AP transmit power for the following

TABLE II: Convergence time comparison.

Design approach	Convergence time (second)									
	$N = 10$		$N = 20$		$N = 30$		$N = 40$		$N = 50$	
	(2, 4)	(4, 8)	(2, 4)	(4, 8)	(2, 4)	(4, 8)	(2, 4)	(4, 8)	(2, 4)	(4, 8)
Penalty-based method	2.8	8.1	3.4	9.2	4.1	10.6	5.3	12.1	6.4	13.6
Two-stage method	0.04	0.07	0.09	0.14	0.14	0.25	0.21	0.40	0.30	0.51

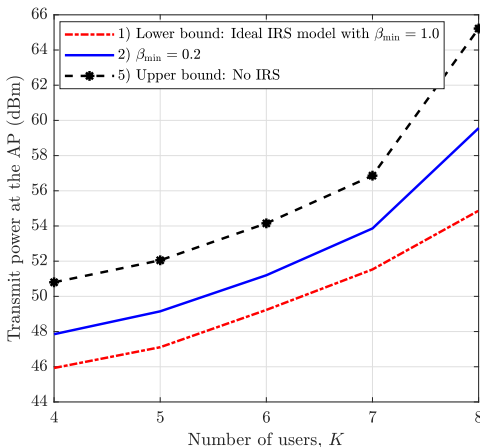


Fig. 11: AP transmit power versus number of users.

schemes:

- 1) Lower bound: solve (P6) with  $\beta_{\min} = 1$  using the extended penalty-based method.
- 2) Solve (P6) with  $\beta_{\min} = 0.2$  using the extended penalty-based method.
- 3) Solve (P7.1) and (P7.1) with  $\beta_{\min} = 0.2$  using the two-stage method.
- 4) Ideal IRS assumption: phase shifts obtained by the extended penalty-based algorithm by assuming  $\beta_{\min} = 1$ , but applied to a practical IRS with  $\beta_{\min} = 0.2$ .
- 5) Upper bound: the system without using an IRS by solving (P7.2) with  $\mathbf{h}_k = \mathbf{h}_{d,k}$ .

It is observed that the performance gap between the extended penalty-based method and two-stage method increases as  $\gamma$  increases. Although the two-stage method suffers from small performance loss in the low SINR regime compared to the extended penalty-based method, it performs even worse than scheme 4) in the high SINR regime. This is because the multiuser interference becomes the performance bottleneck when the user SINR target is high, and thus the joint transmit beamforming and IRS reflect beamforming design becomes more crucial, which requires the use of both the practical phase shift model as well as more sophisticated optimization. However, the low-complexity two-stage algorithm is still beneficial for low SINR targets, e.g.,  $-5$  dB.

Next, in Table II, we compare the average central processing unit (CPU) running time of the extended penalty-based algorithm and two-stage algorithm for different  $(K, M)$  pairs and  $N$ . The simulations are implemented on MATLAB R2017a and tested on a PC with a Core i7-2600 CPU, 8-GB of RAM, and Windows 10. It is observed that the results in Table II are consistent with the complexity analysis presented in Sections V-B and V-C. Specifically, the two-stage algorithm converges

much faster than the extended penalty-based algorithm. This is due to the fact that the two-stage algorithm requires solving two sub-problems, i.e., (P7.1) and (P7.2), for one time only.

In Fig. 11, we show the AP transmit power versus the number of users,  $K$ , by setting  $\gamma_k = 10$  dB,  $M = 8$ , and  $d = 395$  m. In particular, we successively add users to the cluster and obtain the required AP transmit power using the extended-penalty-based method. It is observed that the required transmit power increases from  $K = 4$  to  $K = 7$  while the performance gap between different schemes remains almost constant. However, when the number of users becomes equal to that of antennas at the AP, i.e.,  $K = M = 8$ , the AP transmit power in the case without IRS increases more drastically than that with the ideal IRS assuming  $\beta_{\min} = 1$ . This is due to the fact that adding the 8-th user results in a poorly-conditioned MIMO channel in the case without IRS, while adding the IRS with  $\beta_{\min} = 1$  is able to transform the overall effective MIMO channel to be well-conditioned by adding strong multi-paths via IRS reflection. However, by applying the practical IRS with  $\beta_{\min} = 0.2$ , the IRS reflection is not strong enough to recover the full spatial multiplexing gain and thus results in considerable power loss. This demonstrates that in the multiuser case, the practical phase shift model results in not only lower IRS-reflected signal power but also reduced spatial multiplexing gain.

## VII. CONCLUSION

In this paper, we proposed a practical IRS phase shift model and validated its accuracy based on experimental results. Under this new model, we formulated and solved new joint transmit and reflect beamforming optimization problems in IRS-aided multiuser systems to minimize the transmit power at the AP subject to users' individual SINR constraints, by applying the AO and penalty-based optimization techniques. Our simulation results showed that beamforming optimization based on the conventional ideal phase shift model, albeit having been widely used in the literature, may lead to significant performance loss as compared to the proposed practical model for both the single-user and multiuser setups, especially when the effective resistance of the reflecting circuit is large. In future work, it will be worth investigating such performance difference in more general IRS-aided wireless communication systems, such as OFDM-based system [13], [14], NOMA-based system [15], [16], physical layer security system [7]–[12], and SWIPT system [17]–[19]. Other promising research problems include the channel state information (CSI) acquisition and robust beamforming design with imperfect CSI [44] under the practical IRS phase shift model.

## APPENDIX A: PROOF OF PROPOSITION 1

Since the IRS-reflected signal dominates in the user's receive signal power for asymptotically large  $N$ , the signal from the AP-user link ( $\mathbf{h}_d$ ) can be ignored. Thus,  $P_{\text{practical}}$  is approximately given by  $P_{\text{practical}} \approx P\mathbb{E}(\|(\mathbf{v}^H \text{diag}(\mathbf{h}_r^H)\mathbf{G})\|^2)$ , with  $\mathbf{v}(n) = \beta_n(\theta_n)e^{j\theta_n}$ ,  $\beta_n(\theta_n) = (1 - \beta_{\min})(\frac{\sin(\theta_n - \phi) + 1}{2})^k + \beta_{\min}$ . Let  $\boldsymbol{\theta} = [\theta_1, \dots, \theta_N]$ . When  $M = 1$  and assuming the ideal phase shift model, i.e.,  $\beta_n(\theta_n) = 1, \forall n$  in (15), the optimal solution of  $\boldsymbol{\theta}$  to (P1) is given by  $\theta_n^* = -\arg(\mathbf{G}(n, 1)) + \arg(\mathbf{h}_r(n)), \forall n$  [2]. Then we have

$$\begin{aligned} \|(\mathbf{v}^H \text{diag}(\mathbf{h}_r^H)\mathbf{G})\|^2 &= \left| \left( \sum_{n=1}^N |\mathbf{v}(n)| |\mathbf{h}_r(n)| |\mathbf{G}(n, 1)| \right) \right|^2 \\ &= \left( \sum_{n=1}^N |\mathbf{v}(n)|^2 |\mathbf{h}_r(n)|^2 |\mathbf{G}(n, 1)|^2 \right. \\ &\quad \left. + \sum_{n=1}^N \sum_{i \neq n}^N |\mathbf{v}(n)| |\mathbf{h}_r(n)| |\mathbf{G}(n, 1)| |\mathbf{v}(i)| |\mathbf{h}_r(i)| |\mathbf{G}(i, 1)| \right). \end{aligned} \quad (68)$$

Note that  $|\mathbf{h}_r(n)|$  and  $|\mathbf{G}(n, m)|$  follow Rayleigh distribution with mean values  $\sqrt{\pi}\varrho_r/2$  and  $\sqrt{\pi}\varrho_g/2$ . Since  $|\mathbf{v}(n)|$ ,  $|\mathbf{h}_r(n)|$ , and  $|\mathbf{G}(n, m)|$  are statistically independent, we have

$$\begin{aligned} \mathbb{E}(|\mathbf{v}(n)|^2 |\mathbf{h}_r(n)|^2 |\mathbf{G}(n, 1)|^2) &= \varrho_r^2 \varrho_g^2 \mathbb{E}(|\mathbf{v}(n)|^2) \\ &= \varrho_r^2 \varrho_g^2 \mathbb{E}(\beta_n(\theta_n)^2), \\ \mathbb{E}(|\mathbf{v}(n)| |\mathbf{h}_r(n)| |\mathbf{G}(n, 1)|) &= \frac{\pi \varrho_r \varrho_g \mathbb{E}(|\mathbf{v}(n)|)}{4} \\ &= \frac{\pi \varrho_r \varrho_g \mathbb{E}(\beta_n(\theta_n))}{4}. \end{aligned}$$

It then follows that

$$\begin{aligned} P_{\text{practical}} &= P\mathbb{E}(\|(\mathbf{v}^H \text{diag}(\mathbf{h}_r^H)\mathbf{G})\|^2) \\ &= PN\varrho_r^2 \varrho_g^2 \mathbb{E}(\beta_n(\theta_n)^2) \\ &\quad + PN(N-1) \frac{\pi^2 \varrho_r^2 \varrho_g^2 \mathbb{E}(\beta_n(\theta_n))^2}{16}. \end{aligned}$$

On the other hand, under the same phase shift solution  $\boldsymbol{\theta}$ , for the ideal IRS model with the unity amplitude at each reflecting element regardless of the phase shift, i.e.,  $\beta_n(\theta_n) = 1, \forall n$ , we have

$$P_{\text{ideal}} = PN\varrho_r^2 \varrho_g^2 + PN(N-1) \frac{\pi^2 \varrho_r^2 \varrho_g^2}{16}, \quad (69)$$

since  $\mathbb{E}(\beta_n(\theta_n)^2) = 1$  and  $\mathbb{E}(\beta_n(\theta_n)) = 1$ . The ratio between  $P_{\text{practical}}$  and  $P_{\text{ideal}}$  is thus given by

$$\begin{aligned} \eta(\beta_{\min}, k) &= \frac{P_{\text{practical}}}{P_{\text{ideal}}} \\ &= \frac{\frac{16\mathbb{E}(\beta_n(\theta_n)^2) - \pi^2 \mathbb{E}(\beta_n(\theta_n))^2}{N} + \pi^2 \mathbb{E}(\beta_n(\theta_n))^2}{\frac{16 - \pi^2}{N} + \pi^2}. \end{aligned}$$

When  $N \rightarrow \infty$ ,  $\frac{16\mathbb{E}(\beta_n(\theta_n)^2) - \pi^2 \mathbb{E}(\beta_n(\theta_n))^2}{N} = 0$  and  $\frac{16 - \pi^2}{N} = 0$ . As a result, we have

$$\eta(\beta_{\min}, k) = \mathbb{E}(\beta_n(\theta_n))^2 = \left( \frac{1}{2\pi} \int_{-\pi}^{\pi} \beta(\theta) d\theta \right)^2, \quad (70)$$

with  $\beta(\theta) = (1 - \beta_{\min}) \left( \frac{\sin(\theta - \phi) + 1}{2} \right)^k + \beta_{\min}$ , since  $\theta$  is uniformly distributed in  $[-\pi, \pi]$ . This thus completes the proof.

## APPENDIX B: PROOF OF PROPOSITION 2

Let  $\delta \geq 0$  be a sufficiently small constant. First, considering the case of  $\arg(\varphi_n) \geq 0$  or  $\lambda = 0$ , the following inequalities are obtained:

- Since  $\beta_n(\arg(\varphi_n)) \geq \beta_n(\arg(\varphi_n) - \delta)$  and  $\cos(\delta) \leq 1$ ,  $f(\arg(\varphi_n)) \geq f(\arg(\varphi_n) - \delta)$ .
- Since  $\beta_n(\pi) \geq \beta_n(\pi + \delta)$  and  $\cos(\delta) \leq 1$ ,  $f(\pi) \geq f(\pi + \delta)$ .

It then follows that  $\exists \delta \in [0, \pi - \arg(\varphi_n)]$  such that  $f(\arg(\varphi_n) + \delta) \geq f(\arg(\varphi_n))$  and thus  $\theta_n^* \in [\arg(\varphi_n), \pi]$ . Similarly, we can show  $\theta_n^* \in [\arg(\varphi_n), -\pi]$  when  $\arg(\varphi_n) < 0$  or  $\lambda = 1$ . The proof is thus completed.

## APPENDIX C: PROOF OF PROPOSITION 3

Given three points  $\theta_A, \theta_B, \theta_C$  and their corresponding function values  $f_1, f_2, f_3$ , we seek to determine three constants  $a_0, a_1$ , and  $a_2$  such that the following quadratic function is constructed,

$$g(\theta_n) = a_0 + a_1(\theta_n - \theta_A) + a_2(\theta_n - \theta_A)(\theta_n - \theta_B). \quad (71)$$

When  $\theta_n = \theta_A$ ,  $\theta_n = \theta_B$ , and  $\theta_n = \theta_C$ , the constants  $a_0, a_1$ , and  $a_2$  can be respectively obtained. Substituting them into the stationary point of  $g(\theta_n)$ , i.e.,  $\hat{\theta}_n^* = \frac{\theta_A + \theta_B}{2} - \frac{a_1}{2a_2}$ , allows us to obtain (21). The proof is thus completed.

## APPENDIX D: PROOF OF PROPOSITION 4

Let  $\Delta > 0$ ,  $f(\theta_n) \triangleq 2\beta_n(\theta_n)|v_n| \cos(\psi_n - \theta_n) - \beta_n^2(\theta_n)$ , and  $\lambda = 0$  when  $\psi_n \geq 0$  or  $\lambda = 1$  otherwise. If  $f(\psi_n - \Delta) > f(\psi_n)$  for  $\lambda = 0$ , we have

$$\frac{\beta_n^2(\psi_n) - \beta_n^2(\psi_n - \Delta)}{2(\beta_n(\psi_n) - \beta_n(\psi_n - \Delta) \cos(\Delta))} > |v_n|. \quad (72)$$

Since  $\beta_n(\psi_n) - \beta_n(\psi_n - \Delta) \cos(\Delta) > \beta_n(\psi_n) - \beta_n(\psi_n - \Delta)$ , (72) can be simplified as

$$\frac{\beta_n(\psi_n) + \beta_n(\psi_n - \Delta)}{2} > |v_n|. \quad (73)$$

Likewise, if  $f(\psi_n + \Delta) > f(\psi_n)$  for  $\lambda = 0$ , the following inequality can be obtained similarly by following the above steps.

$$\frac{\beta_n(\psi_n) + \beta_n(\psi_n + \Delta)}{2} < |v_n|. \quad (74)$$

It is not difficult to observe that always  $\exists \Delta$  such that either (73) or (74) holds depending on the values of  $v_n$  and  $\psi_n$ . Following the similar steps as above allows us to obtain (31) for the case of  $\lambda = 1$ . The proof is thus completed.

## REFERENCES

- [1] S. Abeywickrama, R. Zhang, and C. Yuen, "Intelligent reflecting surface: Practical phase shift model and beamforming optimization," [Online]. Available: <https://arxiv.org/abs/1907.06002>.
- [2] Q. Wu and R. Zhang, "Intelligent reflecting surface enhanced wireless network via joint active and passive beamforming," *IEEE Trans. Wireless Commun.*, vol. 18, no. 11, pp. 5394–5409, Nov. 2019.
- [3] Q. Wu and R. Zhang, "Towards smart and reconfigurable environment: Intelligent reflecting surface aided wireless network," *IEEE Commun. Mag.*, vol. 58, no. 1, pp. 106–112, Jan. 2020.
- [4] C. Huang, A. Zappone, G. C. Alexandropoulos, M. Debbah, and C. Yuen, "Reconfigurable intelligent surfaces for energy efficiency in wireless communication," *IEEE Trans. Wireless Commun.*, vol. 18, no. 8, pp. 4157–4170, Aug. 2019.
- [5] E. Basar, M. Di Renzo, J. De Rosny, M. Debbah, M. Alouini, and R. Zhang, "Wireless communications through reconfigurable intelligent surfaces," *IEEE Access*, vol. 7, pp. 116 753–116 773, Aug. 2019.
- [6] C. Huang *et al.*, "Holographic MIMO surfaces for 6G wireless networks: Opportunities, challenges, and trends," [Online]. Available: <https://arxiv.org/abs/1911.12296>.
- [7] M. Cui, G. Zhang, and R. Zhang, "Secure wireless communication via intelligent reflecting surface," *IEEE Wireless Commun. Lett.*, vol. 8, no. 5, pp. 1410–1414, Oct. 2019.
- [8] X. Guan, Q. Wu, and R. Zhang, "Intelligent reflecting surface assisted secrecy communication: Is artificial noise helpful or not?" *IEEE Wireless Commun. Lett.*, DOI:10.1109/LWC.2020.2969629, Jan. 2020.
- [9] D. Xu, X. Yu, Y. Sun, D. W. K. Ng, and R. Schober, "Resource allocation for secure IRS-assisted multiuser MISO systems," [Online]. Available: <https://arxiv.org/abs/1907.03085>.
- [10] Z. Chu, W. Hao, P. Xiao, and J. Shi, "Intelligent reflecting surface aided multi-antenna secure transmission," *IEEE Wireless Commun. Lett.*, vol. 9, no. 1, pp. 108–112, Jan. 2020.
- [11] X. Lu, W. Yang, X. Guan, Q. Wu, and Y. Cai, "Robust and secure beamforming for intelligent reflecting surface aided mmWave MISO systems," [Online]. Available: <https://arxiv.org/abs/2003.11195>.
- [12] H. Yang *et al.*, "Deep reinforcement learning based intelligent reflecting surface for secure wireless communications," [Online]. Available: <https://arxiv.org/abs/2002.12271>.
- [13] Y. Yang, B. Zheng, S. Zhang, and R. Zhang, "Intelligent reflecting surface meets OFDM: Protocol design and rate maximization," *IEEE Trans. on Commun.*, DOI:10.1109/TCOMM.2020.2981458, Mar. 2020.
- [14] B. Zheng and R. Zhang, "Intelligent reflecting surface-enhanced OFDM: Channel estimation and reflection optimization," *IEEE Wireless Commun. Lett.*, vol. 9, no. 4, pp. 518–522, Apr. 2020.
- [15] G. Yang, X. Xu, and Y.-C. Liang, "Intelligent reflecting surface assisted non-orthogonal multiple access," [Online]. Available: <https://arxiv.org/abs/1907.03133>.
- [16] B. Zheng, Q. Wu, and R. Zhang, "Intelligent reflecting surface-assisted multiple access with user pairing: NOMA or OMA?" *IEEE Commun. Lett.*, vol. 24, no. 4, pp. 753–757, Apr. 2020.
- [17] Q. Wu and R. Zhang, "Weighted sum power maximization for intelligent reflecting surface aided SWIPT," *IEEE Wireless Commun. Lett.*, vol. 9, no. 5, pp. 586–590, May 2020.
- [18] Q. Wu and R. Zhang, "Joint active and passive beamforming optimization for intelligent reflecting surface assisted SWIPT under QoS constraints," *to appear in IEEE J. Sel. Areas Commun.*, [Online]. Available: <https://arxiv.org/abs/1910.06220>.
- [19] C. Pan, H. Ren, K. Wang, M. Elkashlan, A. Nallanathan, J. Wang, and L. Hanzo, "Intelligent reflecting surface enhanced MIMO broadcasting for simultaneous wireless information and power transfer," *to appear in IEEE J. Sel. Areas Commun.*, [Online]. Available: <https://arxiv.org/abs/1908.04863>.
- [20] Q.-U.-A. Nadeem, A. Kammoun, A. Chaaban, M. Debbah, and M.-S. Alouini, "Intelligent reflecting surface assisted multi-user MISO communication," [Online]. Available: <https://arxiv.org/abs/1906.02360>.
- [21] P. Wang, J. Fang, and H. Li, "Joint beamforming for intelligent reflecting surface-assisted millimeter wave communications," [Online]. Available: <https://arxiv.org/abs/1910.08541>.
- [22] S. Zhang and R. Zhang, "Capacity characterization for intelligent reflecting surface aided MIMO communication," *to appear in IEEE J. Sel. Areas Commun.*, [Online]. Available: <https://arxiv.org/abs/1910.01573>.
- [23] C. Pan, H. Ren, K. Wang, W. Xu, M. Elkashlan, A. Nallanathan, and L. Hanzo, "Multicell MIMO communications relying on intelligent reflecting surface," [Online]. Available: <https://arxiv.org/abs/1907.10864>.
- [24] M. Fu, Y. Zhou, and Y. Shi, "Intelligent reflecting surface for downlink non-orthogonal multiple access networks," [Online]. Available: <https://arxiv.org/abs/1906.09434>.
- [25] X. Mu, Y. Liu, L. Guo, J. Lin, and N. Al-Dahir, "Exploiting intelligent reflecting surfaces in multi-antenna aided NOMA systems," [Online]. Available: <https://arxiv.org/abs/1910.13636>.
- [26] M.-M. Zhao, Q. Wu, M.-J. Zhao, and R. Zhang, "Intelligent reflecting surface enhanced wireless network: Two-timescale beamforming optimization," [Online]. Available: <https://arxiv.org/abs/1912.01818>.
- [27] X. Guan, Q. Wu, and R. Zhang, "Joint power control and passive beamforming in IRS-assisted spectrum sharing," *IEEE Commun. Lett.*, DOI:10.1109/LCOMM.2020.2979709, Mar. 2020.
- [28] M. Hua *et al.*, "Intelligent reflecting surface-aided joint processing coordinated multipoint transmission," [Online]. Available: <https://arxiv.org/abs/2002.12271>.
- [29] C. Huang, R. Mo, and C. Yuen, "Reconfigurable intelligent surface assisted multiuser MISO systems exploiting deep reinforcement learning," *to appear in IEEE J. Sel. Areas Commun.*, [Online]. Available: <https://arxiv.org/abs/2002.10072>.
- [30] H. Rajagopal and Y. Rahmat-Samii, "Loss quantification for microstrip reflectarray: Issue of high fields and currents," in *Proc. IEEE Antennas and Propag. Society Int. Symposium*, Jul. 2008, pp. 1–4.
- [31] W. Tang *et al.*, "MIMO transmission through reconfigurable intelligent surface: System design, analysis, and implementation," [Online]. Available: <https://arxiv.org/abs/1912.09955>.
- [32] B. O. Zhu, J. Zhao, and Y. Feng, "Active impedance metasurface with full 360 reflection phase tuning," *Scientific reports*, vol. 3, pp. 3059–3064, Oct. 2013.
- [33] M. E. Bialkowski, A. W. Robinson, and H. J. Song, "Design, development, and testing of X-band amplifying reflectarrays," *IEEE Trans. on Antennas and Propag.*, vol. 50, no. 8, pp. 1065–1076, Aug. 2002.
- [34] W. Tang, X. Li, J. Y. Dai, S. Jin, Y. Zeng, Q. Cheng, and T. J. Cui, "Wireless communications with programmable metasurface: Transceiver design and experimental results," [Online]. Available: <https://arxiv.org/abs/1811.08119>.
- [35] F. Liu *et al.*, "Intelligent metasurfaces with continuously tunable local surface impedance for multiple reconfigurable functions," *Phys. Rev. Applied*, vol. 11, no. 4, pp. 44 024–44 033, Apr. 2019.
- [36] S. Koziel and L. Leifsson, *Surrogate-based modeling and optimization*. Springer, 2013.
- [37] D. M. Pozar, *Microwave Engineering (3th Edition)*. New York John Wiley & Sons, 2005.
- [38] R. P. Brent, *Algorithms for Minimization without Derivatives*. Prentice-Hall, 1973.
- [39] Q. Shi, M. Hong, X. Gao, E. Song, Y. Cai, and W. Xu, "Joint source-relay design for full-duplex MIMO AF relay systems," *IEEE Trans. Signal Process.*, vol. 64, no. 23, pp. 6118–6131, Dec. 2016.
- [40] Y. Sun, P. Babu, and D. P. Palomar, "Majorization-minimization algorithms in signal processing, communications, and machine learning," *IEEE Trans. Signal Process.*, vol. 65, no. 3, pp. 794–816, Feb. 2017.
- [41] M. Schubert and H. Boche, "Solution of the multiuser downlink beamforming problem with individual SINR constraints," *IEEE Trans. Veh. Technol.*, vol. 53, no. 1, pp. 18–28, Jan. 2004.
- [42] Z.-Q. Luo and W. Yu, "An introduction to convex optimization for communications and signal processing," *IEEE J. Sel. Areas Commun.*, vol. 24, no. 8, pp. 1426–1438, Aug. 2006.
- [43] Q. Wu and R. Zhang, "Beamforming optimization for wireless network aided by intelligent reflecting surface with discrete phase shifts," *IEEE Trans. on Commun.*, vol. 68, no. 3, pp. 1838–1851, Mar. 2020.
- [44] G. Zhou, C. Pan, H. Ren, K. Wang, and A. Nallanathan, "A framework of robust transmission design for IRS-aided MISO communications with imperfect cascaded channels," [Online]. Available: <https://arxiv.org/abs/2001.07054>.



**Samith Abeywickrama** (S'16) received the B. Sc. degree in electronic and telecommunication engineering from the University of Moratuwa, Sri Lanka, in 2016. He is currently pursuing the Ph.D. degree with the Department of Electrical and Computer Engineering at National University of Singapore, Singapore, and Singapore University of Technology and Design, Singapore. His research interests include intelligent reflecting surface (IRS), wireless power transfer, and localization.



**Rui Zhang** (S'00-M'07-SM'15-F'17) received the B.Eng. (first-class Hons.) and M.Eng. degrees from the National University of Singapore, Singapore, and the Ph.D. degree from the Stanford University, Stanford, CA, USA, all in electrical engineering.

From 2007 to 2010, he worked at the Institute for Infocomm Research, ASTAR, Singapore. Since 2010, he has been working with the National University of Singapore, where he is now a Professor in the Department of Electrical and Computer Engineering. He has published over 200 journal papers and over 180 conference papers. He has been listed as a Highly Cited Researcher by Thomson Reuters/Clarivate Analytics since 2015. His current research interests include UAV/satellite communications, wireless power transfer, reconfigurable MIMO, and optimization methods.

He was the recipient of the 6th IEEE Communications Society Asia-Pacific Region Best Young Researcher Award in 2011, and the Young Researcher Award of National University of Singapore in 2015. He was the co-recipient of the IEEE Marconi Prize Paper Award in Wireless Communications in 2015 and 2020, the IEEE Communications Society Asia-Pacific Region Best Paper Award in 2016, the IEEE Signal Processing Society Best Paper Award in 2016, the IEEE Communications Society Heinrich Hertz Prize Paper Award in 2017 and 2020, the IEEE Signal Processing Society Donald G. Fink Overview Paper Award in 2017, and the IEEE Technical Committee on Green Communications & Computing (TCGCC) Best Journal Paper Award in 2017. His co-authored paper received the IEEE Signal Processing Society Young Author Best Paper Award in 2017. He served for over 30 international conferences as the TPC co-chair or an organizing committee member, and as the guest editor for 3 special issues in the IEEE JOURNAL OF SELECTED TOPICS IN SIGNAL PROCESSING and the IEEE JOURNAL ON SELECTED AREAS IN COMMUNICATIONS. He was an elected member of the IEEE Signal Processing Society SPCOM Technical Committee from 2012 to 2017 and SAM Technical Committee from 2013 to 2015, and served as the Vice Chair of the IEEE Communications Society Asia-Pacific Board Technical Affairs Committee from 2014 to 2015. He served as an Editor for the IEEE TRANSACTIONS ON WIRELESS COMMUNICATIONS from 2012 to 2016, the IEEE JOURNAL ON SELECTED AREAS IN COMMUNICATIONS: Green Communications and Networking Series from 2015 to 2016, and the IEEE TRANSACTIONS ON SIGNAL PROCESSING from 2013 to 2017. He is now an Editor for the IEEE TRANSACTIONS ON COMMUNICATIONS and the IEEE TRANSACTIONS ON GREEN COMMUNICATIONS AND NETWORKING. He serves as a member of the Steering Committee of the IEEE Wireless Communications Letters. He is a Distinguished Lecturer of IEEE Signal Processing Society and IEEE Communications Society.



**Qingqing Wu** (S'13-M'16) received the B.Eng. and the Ph.D. degrees in Electronic Engineering from South China University of Technology and Shanghai Jiao Tong University (SJTU) in 2012 and 2016, respectively. He is currently an assistant professor in the Department of Electrical and Computer Engineering at the University of Macau, China, and also affiliated with the State key laboratory of Internet of Things for Smart City. From 2016 to 2020, he was a Research Fellow in the Department of Electrical and Computer Engineering at National University of Singapore. His current research interest includes intelligent reflecting surface (IRS), unmanned aerial vehicle (UAV) communications, and MIMO transceiver design. He has published over 60 IEEE journal and conference papers.

He was the recipient of the IEEE WCSP Best Paper Award in 2015, the Outstanding Ph.D. Thesis Funding in SJTU in 2016, the Outstanding Ph.D. Thesis Award of China Institute of Communications in 2017. He was the Exemplary Editor of IEEE Communications Letters in 2019 and the Exemplary Reviewer of several IEEE journals. He serves as an Associate Editor for IEEE Communications Letters and IEEE Open Journal of Communications Society. He is the Lead Guest Editor for IEEE Journal on Selected Areas in Communications on "UAV Communications in 5G and Beyond Networks", and the Guest Editor for IEEE Open Journal on Vehicular Technology on "6G Intelligent Communications" and IEEE Open Journal of Communications Society on "Reconfigurable Intelligent Surface-Based Communications for 6G Wireless Networks". He is the workshop co-chair for ICC 2019 and ICC 2020 workshop on "Integrating UAVs into 5G and Beyond", and the workshop co-chair for GLOBECOM 2020 workshop on "Reconfigurable Intelligent Surfaces for Wireless Communication for Beyond 5G".



**Chau Yuen** (S'04-M'06-SM'12) received the B.Eng. and Ph.D. degrees from Nanyang Technological University (NTU), Singapore, in 2000 and 2004, respectively. He was a Post-Doctoral Fellow with Lucent Technologies Bell Labs, Murray Hill, in 2005. He was a Visiting Assistant Professor with The Hong Kong Polytechnic University in 2008. From 2006 to 2010, he was a Senior Research Engineer with the Institute for Infocomm Research (I2R), Singapore, where he was involved in an industrial project on developing an 802.11n Wireless LAN system and participated actively in 3Gpp long-term evolution (LTE) and LTE-advanced (LTE-A) standardization. Since 2010, he has been with the Singapore University of Technology and Design.

Dr. Yuen was a recipient of the Lee Kuan Yew Gold Medal, the Institution of Electrical Engineers Book Prize, the Institute of Engineering of Singapore Gold Medal, and the Merck Sharp and Dohme Gold Medal, and he was twice a recipient of the Hewlett Packard Prize. He received the IEEE AsiaPacific Outstanding Young Researcher Award in 2012. He serves as an Editor for the IEEE TRANSACTIONS ON COMMUNICATIONS and the IEEE TRANSACTIONS ON VEHICULAR TECHNOLOGY, and awarded as the Top Associate Editor from 2009 to 2015.